UPPSALA
UNIVERSITET

Digital Comprehensive Summaries of Uppsala Dissertations from the Faculty of Science and Technology 547

Direct Driven Generators for Vertical Axis Wind Turbines

SANDRA ERIKSSON

ACTA
UNIVERSITATIS
UPSALIENSIS
UPPSALA
2008

ISSN 1651-6214
ISBN 978-91-554-7264-1
urn:nbn:se:uu:diva-9210

Dissertation presented at Uppsala University to be publicly examined in Polhemsalen, Ångströmlaboratoriet, Lägerhyddsvägen 1, Uppsala, Friday, September 26, 2008 at 13:15 for the degree of Doctor of Philosophy. The examination will be conducted in English.

Abstract
Eriksson, S. 2008. Direct Driven Generators for Vertical Axis Wind Turbines. Acta Universitatis Upsaliensis. *Digital Comprehensive Summaries of Uppsala Dissertations from the Faculty of Science and Technology* 547. 88 pp. Uppsala. ISBN 978-91-554-7264-1.

Wind power is a renewable energy source that is increasingly used all over the world. Most wind turbines have a horizontal axis of rotation but a few have a vertical axis of rotation. The concept presented in this thesis is a straight-bladed vertical axis wind turbine with a direct driven cable-wound permanent magnet synchronous generator. A comparison of the two different types of wind turbines, vertical axis wind turbines and horizontal axis wind turbines, have been performed considering several different aspects. However, the main focus in this thesis is on the generator.

Several generators have been modelled with a combined field and circuit model, which has been solved by using the finite element method. A 12 kW generator has been designed, which has a high overall efficiency and a high overload capability. The generator has been constructed at the department and was tested in the laboratory before being mounted in a vertical axis wind turbine. Results from experiments correspond well with results from simulations. The generator has been tested for different loading conditions and the harmonic content of the voltage has been analysed. A 12 kW vertical axis wind turbine was completed and tests have been performed. The results are encouraging and further studies on the prototype will be performed in the future.

The simulation method has been used to study electromagnetic losses in several generators. The comparison showed that the average losses should be considered when a variable speed generator for wind power is designed and it concluded that the design optimization process becomes a compromise between lowering the electromagnetic losses and having high overload capability.

When constructing a wind turbine, it is important to consider vibrations in the structure. Torsional vibrations in the drive shaft connecting the turbine to the rotor of the generator have been studied. It is shown that a direct driven generator is to prefer over an induction generator with a gearbox when torsional vibrations are concerned.

This thesis is based on eight papers all concerning vertical axis wind turbines with three of them focusing on the generator.

Keywords: synchronous generator, wind power, vertical axis wind turbine, simulations, experiments, finite element method

Sandra Eriksson, Department of Engineering Sciences, Box 534, Uppsala University, SE-75121 Uppsala, Sweden

ISSN 1651-6214
ISBN 978-91-554-7264-1
urn:nbn:se:uu:diva-9210 (http://urn.kb.se/resolve?urn=urn:nbn:se:uu:diva-9210)

List of Papers

This thesis is based on the following papers, which are referred to in the text by their Roman numerals.

I **S. Eriksson**, H. Bernhoff and M. Leijon. Evaluation of different turbine concepts for wind power. *Renewable and Sustainable Energy Reviews*, 12(5):1419-1434, 2008.

II **S. Eriksson** and H. Bernhoff. Generator-damped torsional vibrations of a vertical axis wind turbine. *Wind Engineering*, 29(5): 449-462, 2005.

III A. Solum, P. Deglaire, **S. Eriksson**, M. Stålberg, M. Leijon and H. Bernhoff. Design of a 12kW vertical axis wind turbine equipped with a direct driven PM synchronous generator. *EWEC 2006 - European Wind Energy Conference & Exhibition*, Athens, Greece.

IV P. Deglaire, **S. Eriksson**, J. Kjellin and H. Bernhoff. Experimental results from a 12 kW vertical axis wind turbine with a direct driven PM synchronous generator. *EWEC 2007 - European Wind Energy Conference & Exhibition*, Milan, Italy.

V J. Kjellin, **S. Eriksson**, P. Deglaire, F. Bülow and H. Bernhoff. Progress of control system and measurement techniques for a 12 kW vertical axis wind turbine. *Scientific proceedings of EWEC 2008 - European Wind Energy Conference & Exhibition*:186-190.

VI **S. Eriksson**, A. Solum, M. Leijon and H. Bernhoff. Simulations and experiments on a 12 kW direct driven PM synchronous generator for wind power. *Renewable Energy*, 33(4):674-681, 2008.

VII **S. Eriksson**, H. Bernhoff and M. Leijon. FEM simulations and experiments of different loading conditions for a 12 kW direct driven PM synchronous generator for wind power. Conditionally accepted for publication in *International Journal of Emerging Electric Power Systems*.

VIII **S. Eriksson** and H. Bernhoff. Loss evaluation and design optimization for direct driven permanent magnet synchronous generators for wind power. Submitted to *IEEE Transactions on Energy Conversion*, July 2008.

Contents

Nomenclature and abbreviations

$\mathbf{A}$	Tm	Magnetic potential	k_0	Nm/rad	Rotational stiffness
A_{airgap}	m^2	Area in airgap	l	m	Cable length
A_c	Tm	Magn. pot. at bound.	L_s^{end}	H	Coil end inductance
A_{Cu}	m^2	Cable area	M	Nm	Torque
A_t	m^2	Cross section area	M_0	Nm	Torque amplitude
$\mathbf{B}$	T	Magn. flux density	n	-	Gear ratio
B_{eff}	T	Eff. magn. flux dens.	N	-	No. of turns
B_{max}	T	Max.magn.flux dens.	N_B	-	No. of blades
B_r	T	Remanence	$p(v)$	s/m	Probability dens. fcn.
c	Nms/rad	Damping constant	P	W	Power
d	m	Sheet thickness	P_{el}	W	Electric power
c_0	m	Chord length	P_{loss}	W	Power losses
C_P	-	Power coeff.	P_{loss}^{ed},P_{loss}^{ex},		
$\mathbf{D}$	C/m^2	Displacement field	P_{loss}^{hy},P_{loss}^{rot}	W/m^3	Diff. iron losses
$\mathbf{E}$	V/m	Electric field	P_{loss}^{Fe},P_{loss}^{Cu}	W	Diff. losses
E_i	V	No load voltage	$P_{loss}^{Cu,ed}$	W	Cu losses (eddies)
f	Hz	Electric frequency	Q	VAr	Reactive power
f_{dd},f_g	Hz	Rotational freq.	R_i	Ω	Inner resistance
$f_{e,dd}$,$f_{e,g}$	Hz	Eigen frequencies	R_L	Ω	Load resistance
h_{pm}	m	Magnet height	R_0	m	Turbine radius
$\mathbf{H}$	A/m	Magnetic field	s	m	Airgap length
H_c	A/m	Coercivity	S	VA	Apparent power
I	A	Current	t	s	Time
I_{pm}	A	Coil current (PM)	TSR	-	Tip speed ratio
J_0	A/m^2	Current dens. (cable)	U	V	Voltage
$\mathbf{J}_f$	A/m^2	Free current density	U_i	V	Voltage amplitudes
J_m	kgm^2	Mass mom. of in.	v	m/s	Wind speed
$J_{m,eq}$	kgm^2	Equiv.mass mom.	V_s	m^3	Volume
J_{pm}	A/m^2	Coil Current dens.	V	V	Electric potential
k_h,k_{eddy},k_e	n.a.	Loss coefficients	W_E	J	Magnetic energy
k_f	-	Stacking factor	X_d	Ω	Machine reactance

γ	rad	Phase angle	$\sigma_{0,\mathrm{HAWT}}$	-	HAWT solidity
δ	rad	Load angle	$\sigma_{0,\mathrm{VAWT}}$	-	VAWT solidity
δ_s	m	Skin depth	τ	m^3	Volume
η_{el}	-	Electric efficiency	ϕ	Wb	Magnetic flux
θ	rad	Angular displacement	φ	rad	Power factor angle
			$\cos\varphi$	-	Power factor
μ	Vs/Am	Permeability	ω	rad/s	Angular frequency
ξ	-	Damping ratio	ω_d	rad/s	Eigen frequency (damped)
ρ	kg/m^3	Density			
ρ_f	C/m^3	Free charge density	ω_{el}	rad/s	Electric frequency
σ	A/Vm	Conductivity	ω_n	rad/s	Eigen frequency
σ_0	-	Solidity	ω_{mech}	rad/s	Rotational frequency

AC	Alternating Current	PM	Permanent Magnet
DAQ	Data Acquisition	PMSG	Permanent Magnet Synchronous Generator
DC	Direct Current		
FEM	Finite Element Method	p.u.	per unit
HAWT	Horizontal Axis Wind Turbine	rms	root mean square
		TSR	Tip Speed Ratio
IG	Induction Generator	VAWT	Vertical Axis Wind Turbine

1. Introduction

A wish to make better use of the freely available energy sources surrounding us spurs an increasing interest in renewable energy sources such as wind power, solar power, marine current power and wave power. This thesis deals with wind power.

There are a few issues to worry about regarding the future energy production in the world. The most obvious concern is the society's dependence of oil. Different estimations have been presented on when the oil will start to deplete or become too expensive to extract [1]. The need for oil makes countries with no domestic oil-sources more dependent on politically insecure states, such as several of the countries in the Middle East, where a large amount of the known oil reserves exist. However, the most acute problem with the large oil consumption in the world is not the end of the resource but rather the environmental concerns associated with oil, i.e. the greenhouse effect. The greenhouse effect is also contributed to by the coal power. The old coal plants discharge large amounts of carbon dioxide, the dominating greenhouse gas. The greenhouse effect and the climate threat have been discussed substantially during the last years and the discussions were spurred by the report by the International Panel on Climate Change (IPCC) from 2007 stating that the climate change noticed in the last 50 years very likely is due to increased emissions caused by human activity [2].

Another issue, debated in Sweden, is the future of nuclear power. Nuclear power is an energy source without any immediate discharges and is therefore a good energy source when the greenhouse effect is considered. However, a nuclear plant accident could be catastrophic and give a large environmental impact. Furthermore, the ethical right to leave nuclear waste for future generations is debated.

More electricity needs to be produced as the electricity consumption in the world increases. Wind power and other renewable energy sources are an alternative to increasing the use of environmentally damaging energy sources. Wind power is an established form of renewable energy with an installed capacity of almost 20 000 MW in the world, covering about 1 per cent of the global electricity consumption in 2007 [3]. Countries like Denmark and Germany receive a large part of their electricity from wind power. In 2007 wind power covered 21.7 per cent of the Danish electricity consumption[1]. In

[1] http://www.windpower.org/composite-105.htm, Danish Wind Industry Association 2008-07-31

Sweden plans have been made to increase the number of wind turbines substantially. In 2007 Swedish wind turbines produced 1.4 TWh electricity[2]. The Swedish goal[2] is to facilitate the planning and installation of wind turbines producing 10 TWh electricity yearly in 2015. In March 2007, the European leaders set a goal for the European Union of having 20 per cent of the energy supply coming from renewable energy sources[3] such as biomass, hydropower and wind power etc, by 2020. In 2005, 8.5 per cent of the energy in EU[3] came from renewable energy sources.

The wind resource in the world is large. According to a study by the European Wind Energy Association, the total available wind resource that is technically recoverable is 53 000 TWh per year [4], 3.4 times the world's entire electricity consumption[4] in 2005. The world's wind resources are therefore unlikely to be a limiting factor in the utilisation of wind power for electricity generation.

The many different types of wind turbines can be divided into two groups of turbines depending on the orientation of their axis of rotation, namely the most common horizontal axis wind turbines (HAWTs) and vertical axis wind turbines (VAWTs).

1.1 Aim of the thesis

Direct driven permanent magnet synchronous generators for vertical axis wind turbines are studied in this thesis. The aim has been to get increased understanding of how this type of generator works with a VAWT, to verify the numerical model for this type of electrical machine, to study generator design and design optimization and to show that a VAWT with this type of generator can be controlled by the generator. The goal was to increase the understanding of this wind turbine concept in general and the generator in particular, especially from an electromagnetic point of view.

The method has been to design and construct a generator, currently used together with a VAWT and to perform experiments to verify simulations. Emphasis was given to the electromagnetic design process and experimental verification. The simulations were performed by a method where field and circuit equations are combined and solved by using the finite element method.

The work within the wind power group at the division for electricity has been performed as a team, especially concerning the experimental setups. A system approach has been applied on the whole wind turbine, i.e. each part has not been optimized separately but as a part of a whole turbine. The generator has been designed to work with a particular variable speed wind turbine at a chosen site with specified wind resources. The grid interface and the electrical

[2] http://www.regeringen.se/sb/d/2448/a/47768 2008-07-31

[3] http://www.energy.eu/#energy-focus 2008-07-31

[4] http://www.eia.doe.gov/iea/elec.html 2008-07-31

system properties for the suggested wind turbine design are not covered in this thesis. Apart from the work included in this thesis, two papers on aerodynamics [5, 6], a study on thermal overloading of the generator [7] and a licentiate thesis [8] have been made within this project.

The purpose of studying the VAWT is to better understand if it can be an alternative to the HAWT in a longer time perspective. There are several apparent advantages with a VAWT design. For instance it could have a simple design and has potentially a lower investment cost, a high drive train efficiency and requires little maintenance.

1.2 Outline of the thesis

The thesis is based on eight papers with the aim to give a context and a summary of the papers. The thesis is divided into different sections. This first chapter gives an introduction to wind energy and presents the VAWT concept studied in the thesis. The second chapter gives the background to VAWTs, the PM synchronous generator and the simulation method, as well as presenting some current VAWT projects.

The third chapter gives the theoretical background to the papers and the fourth chapter presents the method used in this work, by presenting the simulation method and the experiments.

The fifth chapter gives a summary of the most important results and a discussion, chapter six presents conclusions drawn from this work and chapter seven gives some suggestions for future work. Finally, chapter eight consists of a summary of the included papers.

The eight papers are attached to the thesis as appendices. The first paper is a review and a comparison between VAWTs and HAWTs. The second is a dynamic study of the drive shaft in a VAWT. Paper III to V are conference papers introducing the design, construction and experimental results of a small VAWT. Paper VI to VIII focus on the generator, where paper VI and VII compare experimental results to simulations and paper VIII is a theoretical study of electromagnetic losses in the generator.

1.3 The concept

1.3.1 Turbine

The studied wind energy converter is a VAWT, which is a less common type of wind turbine. The VAWT is omni-directional, i.e. it accepts wind from all directions and does not need a yawing mechanism. In addition, the VAWT is expected to produce less noise than a HAWT [9]. The studied concept has a turbine with straight blades, which are attached to the drive shaft via support arms. This configuration is commonly called an H-rotor, see fig. 1.1. The

drive shaft, usually secluded by a tower or supported by guy wires, is directly connected to the rotor of the generator. A comparison between HAWTs and VAWTs can be found in paper I.

Figure 1.1: An H-rotor.

Simplicity is the main advantage with this wind turbine concept. The wind turbine consists of few parts and will only have one rotating part. The omission of the gearbox, yawing system and pitch system is expected to reduce maintenance [10]. The blades will be fixed, i.e. it will not be possible to turn them out of the wind. The absorbed power will be controlled by an electrical control system combined with passive stall control, i.e. the blades will be designed to stall to limit power absorption at high wind speeds.

The vertical rotational axis of a VAWT allows the generator to be located at the bottom of the tower. This is expected to simplify installation and maintenance. The tower can be lighter for a VAWT since the nacelle is excluded, which reduces structural loads and problems with erecting the tower [11]. The generator design can be focused on efficiency, cost and minimizing maintenance, as the size of the generator is not the main concern. Furthermore, the control system can also be located at ground level facilitating access [12].

There is an apparent difference in the drive train between a HAWT and a VAWT with a ground based generator (apart from turbine configuration): the length of the drive shaft. The long drive shaft of this type of VAWT is interesting to study. However, the long drive shaft is not unique for this system; it has also been used in hydropower. In Järnvägsforsen, Sweden, a hydropower station with two turbine-generator systems of the long shaft type is installed, each having a rated power of 60 MVA, a drive shaft length of 45 meters and a shaft outer diameter of 1.4 meters [13].

1.3.2 Generator

The generator is an important component in a wind turbine, since it converts the mechanical energy in the rotating wind turbine to electricity. In this work, the design strategy of adapting the generator to the turbine has been chosen. The turbine is designed with respect to the desired control strategy and the wind conditions at a planned site. In this concept, the generator will not only be used for energy conversion but it will also electrically control the turbine rotational speed and thus turbine power absorption through stall control. Therefore, the generator have to be strong and robust, which also means that it have to be rather large.

The turbine is connected, through a shaft directly to the rotor of the generator, i.e. the generator is direct driven. The generator will have a slow rotational speed compared to conventional generators. The generator is therefore designed with a large number of poles in order to achieve good induction and high efficiency. Direct drive eliminates losses, maintenance and costs associated with a gearbox. A case study has shown that the gearbox is the part in a wind turbine responsible for most downtime due to failures [10]. Furthermore, the direct drive reduces the torsional constraints on the drive shaft imposed by eigen frequency oscillations, see paper II. Thereby it enables the shaft to be slimmer than if a gearbox had been used, which for an H-rotor means that the supporting tower mass also can be reduced. Gearless wind turbines are becoming increasingly popular [14]. Since a direct driven machine is more bulky and has a larger diameter than a conventional generator there are potential advantages in using a vertical axis turbine and placing the generator on the ground, where the size and weight issue is not of structural concern.

The direct driven generator will deliver an output with a varying voltage level and a varying frequency. Therefore, a full converter is needed as an interface to the grid. The system layout for the permanent magnet synchronous generator (PMSG) and for a conventional induction generator (IG) can be seen in fig. 1.2. The grid interface and system properties for the suggested wind turbine design will not be covered in this thesis, but will be similar to the system described in [15].

The generator's rotor will have permanent magnets (PMs) instead of electromagnets, which is motivated by the simpler rotor construction, i.e. no field coils have to be electrified. Furthermore, the efficiency is improved, as rotor losses are practically eliminated. However, the disadvantage is that the magnetization is constant and not controllable. The PMs are surface-mounted, high-energy magnets made of Neodymium-Iron-Boron [16]. The magnets are chosen to be wide and flat, since the wide magnets decrease the amount of inactive area in the airgap and thereby reduce generator size. The magnets are as wide as possible without getting too much leakage flux between the adjacent magnets. An example of a generator layout can be seen in fig. 1.3.

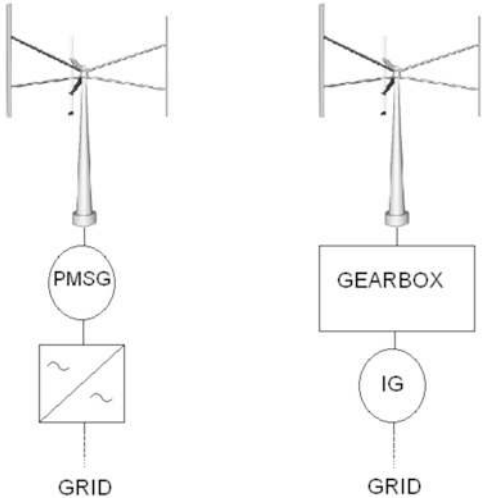

Figure 1.2: System layout for a direct driven permanent magnet synchronous generator (PMSG) to the left and for an induction generator (IG) to the right.

The stator winding consists of circular cables, instead of rectangular conductors, which are commonly used in generators. In rectangular conductors, high electric field strength is reached in the corners, which is avoided in circular cables [17]. The cables normally consist of several copper strands. The cables have been selected to allow the generator to handle a higher current and also a higher voltage than rated. The turbine's power absorption can thereby be controlled electrically, which is important in strong and gusty winds. This electrical power control makes an active mechanical power control of the wind turbine, such as pitch control, superfluous.

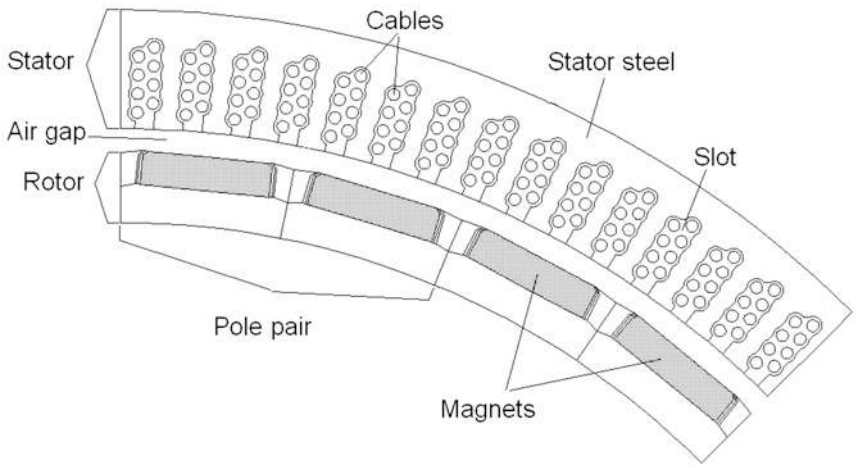

Figure 1.3: Part of a generator.

A cable-wound generator enables the use of higher operating voltage than for traditionally wound machines. For large scale generators the main advantage with high voltage is the possibility to reduce or exclude a transformer from the system [15]. A more efficient system is accomplished, by reducing resistive losses (by having low current) and excluding losses in the transformer as well as losses in the gearbox. Furthermore, a simpler system with fewer parts is expected to require less maintenance, which would reduce the operational costs.

2. Background

2.1 Historical overview of wind power and VAWTs

In this section a short historical overview of wind power with emphasis on the development of VAWTs is presented. For an overview of the status of wind power in 2002, mainly focusing on HAWTs, see [18]. For an overview of wind turbine technologies with emphasis on HAWTs, see [19]. A review of the development of horizontal and vertical axis wind turbines can be found in [20]. VAWTs have during the last years received attention in several journals, see [21–24].

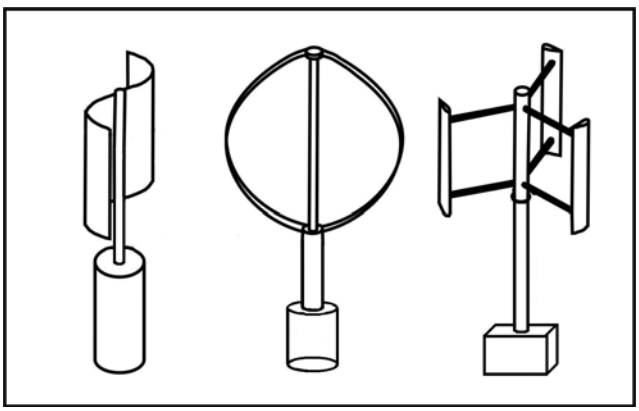

Figure 2.1: Basic VAWT configurations. To the left is a Savonius rotor, in the middle is a Darrieus rotor and to the right is a straight-bladed Darrieus rotor also known as an H-rotor.

The wind has been used as an energy source for a very long time for example in sailing boats. The first windmills were used by the Persians approximately 900 AD. These first windmills were vertical axis wind turbines. During the Middle Ages horizontal axis windmills were built in Europe and used for mechanical tasks such as pumping water or grinding grain. These were the classical four bladed windmills that had a yawing system and were mounted on a big structure. These windmills lost popularity after the industrial revolution. At about the same time water pumping windmills became popular in the United States, recognizable for their many blades and typically situated on a farm. [26]

One of the first attempts to generate electricity by using the wind was made in the United States by Charles Brush in 1888. Among the most important

Figure 2.2: A Sandia turbine with 34 m diameter [25].

early turbines was the turbine developed by Marcellus Jacobs. Jacobs' turbine had three airfoil shaped blades, a battery storage and a wind wane keeping the turbine facing the wind. During the 20th century the horizontal axis wind turbines continued to evolve, which resulted in bigger and more advanced turbines, leading to the modern horizontal axis wind turbines. [26]

Vertical axis wind turbines have been developed in parallel with HAWTs, but with less financial support and less interest. The Finnish engineer S.J. Savonius invented the Savonius turbine in 1922, see fig. 2.1 [27]. In 1931 Georges Darrieus patented his idea to have a vertical axis wind turbine with straight or bent lifting blades, see fig. 2.1 [28].

During the 70's and 80's vertical axis machines came back into focus when both Canada and the United States built several prototypes of Darrieus turbines, see fig. 2.2, which proved to be quite efficient and reliable [22]. However, according to a report from Sandia National Laboratories (USA), the VAWTs fell victims to the poor wind energy market in the USA [29]. The last of the Sandia VAWTs was dismantled in 1997 after cracks had been found in its foundation. In the 80's the American company FloWind commercialized the Darrieus turbine and built several wind farms [30], see fig. 2.3. The machines worked efficiently but had problems with fatigue of the blades, which were designed to flex [31]. More than 500 commercial VAWTs were operating

Figure 2.3: A FloWind wind farm [25].

in California in the mid 80's [25]. The Eole, a 96 meters tall Darrieus turbine built in 1986, is the largest VAWT ever constructed with a rated maximum power of 3.8 MW [32]. The North American Darrieus turbines used in the 80's mostly had induction generators with gearboxes. However, the Eole had a direct driven generator with a diameter of 12 meters. It produced 12 GWh of electric energy during the five years it was running and reached power levels of up to 2.7 MW. The machine was shut down in 1993 due to failure of the bottom bearing.

The straight-bladed VAWT was also an invention included in the original Darrieus patent [28]. This turbine is usually referred to as the straight-bladed Darrieus turbine or the H-rotor, but has also been called giromill or cycloturbine (different concepts of the same invention). In the United Kingdom the H-rotor was investigated by a research team led by Peter Musgrove [23, 33, 34]. The biggest H-rotor built in the U.K. was a 500 kW machine, which was designed in 1989 [35]. This machine had a gearbox and an induction generator inside the top of the tower. One of the machines had blades that could be folded in high wind speeds, see fig. 2.4[1,2]. In the 90's the German company Heidelberg Motor GmbH worked with development of H-rotors and they built several 300 kW prototypes [36, 37], see fig. 2.4[1,2]. These turbines had direct driven generators with large diameters. In some turbines the generator was placed on top of the tower as seen in fig. 2.4[1,2], and in some turbines the generator was situated on the ground.

[1] http://www.hvirvelvinden.dk 2008-08-13

[2] http://www.ifb.uni-stuttgart.de/∼doerner/Darrieus.html 2008-08-01

Figure 2.4: To the left is an H-rotor developed in the U.K. and to the right is one of the Heidelberg rotors.

From this short historical review it is clear that the first windmill was a VAWT but that later HAWTs received most attention.

2.2 Current VAWT projects

The University based research on VAWTs is very limited. Today development of VAWTs is most common in the many small companies producing and marketing small VAWTs.

There is a large number of commercial companies developing small VAWTs. Two research teams, working with turbine geometries somewhere between the Darrieus turbine and the H-rotor, have commercialized their products, both rated at a few kW. The first turbine, called Wind-Sail[3], is Russian. The second turbine is called Turby[4] and is from the Netherlands, see fig. 2.5[4] and [38]. Turby is developed in collaboration with the Technical University in Delft. The Finnish company Windside[5] sells curved Savonius rotors with a special appearance. Another company is Ropatec[6], which sells VAWTs of different configurations with the largest with a rated power of 20 kW and five straight blades. Ropatec has had serial production of their products since 2001 and a worldwide market has been addressed. There are

[3] http://www.wind-sail.com 2008-08-01
[4] http://www.turby.nl 2008-08-01
[5] http://www.windside.com 2008-08-01
[6] http://www.ropatec.com 2008-08-01

Figure 2.5: Turby

several companies[7,8,9,10,11,12] selling small wind turbines similar to the H-rotor. Only a few of them are referred to here.

There are also a few companies focusing on larger VAWTs. A North American company[13] sells Darrieus turbines rated at 200 kW. Another American company sells multi-bladed H-rotors with a rating of up to 4MW [14]. Furthermore, a Chinese company[15] markets VAWTs of different sizes with a rating of up to 3 MW.

2.3 Generator

There are several types of generators available for wind turbines. According to a study of the world market share of wind turbine concepts in the years 1998 to 2002, induction machines dominate the market for wind power generation, but the fixed speed, squirrel cage induction generator is slowly being replaced by the variable speed, doubly-fed induction generator [39]. The use of the synchronous generator is slowly increasing as well and it had a world market share of about 20 per cent in 2002 [39]. Germany's market leading manufacturer of wind turbines, Enercon[16], uses direct driven synchronous electro-

[7] http://www.pacwind.net 2008-08-03
[8] http://www.quietrevolution.co.uk 2008-08-03
[9] http://www.alvestaenergy.com/news.php 2008-08-03
[10] http://www.energycreationuk.co.uk 2008-08-03
[11] http://www.neuhaeuser.com 2008-08-03
[12] http://www.vweltd.co.uk 2008-08-01
[13] http://web.mckenziebay.com 2008-08-01
[14] http://www.fswturbines.com/giromill.html 2008-08-01
[15] http://www.vawtmuce.com 2008-08-04
[16] http://www.enercon.de 2008-08-03

magnetized generators and had a market share of 14 per cent in 2007 [3]. Another German company, Vensys[17], manufactures wind turbines in the MW-range with PM generators [40]. The market share for direct driven PM synchronous generators was less than one per cent in 2006 but it is slowly increasing [40]. Historically PMs have been very expensive but the price has decreased over the last years, which makes it economically viable to use them. Permanent magnet machines are especially common in small wind turbines. Several studies have been conducted on direct driven PM synchronous generators, see [41–45]. Furthermore, several studies of iron losses in wind turbine generators have been made [44–48]. A more extensive overview of different electrical conversion systems for wind turbines can be found in [49].

In 2000, the company ABB made an attempt to commercialize a large, direct driven PM synchronous generator with a cable wound stator for wind power. The invention was called Windformer and was based on the Powerformer technology [15,17,50]. Several of the recently launched generators for wind power generation use a similar technology with few components, direct drive and permanent magnets, see for instance [40].

The generator presented here is a radial flux machine but other designs have been used for wind turbines, for instance axial flux machines and outer rotor designs [51–53]. Furthermore, innovative designs, for instance to have an ironless stator, have been suggested [54].

2.4 The Finite Element Method

The finite element method (FEM) is a numerical method to solve partial differential equations or integral equations. FEM is commonly used in areas such as electromagnetism, structural mechanics etc. where complex sets of equations need to be solved in a simplified way. The method is based on division of the geometry into small triangular parts for a two-dimensional problem. The sets of equations are solved in each little element, where they can be simplified due to the finite geometry.

The finite element method has many roots and has been developed by several researchers in parallel, for instance Turner *et al.*, who published a paper in 1956 [55,56]. FEM was first used to solve problems in structural mechanics in the 1940s and 1950s. Among the first published papers on FEM were work by Argryris (1965) [57] and Marcal *et al.* (1967) [56, 58]. Some important early work was also made by Clough, who is known for having named the method in 1960 [59, 60]. Hannalla and Macdonald [61] were the first to couple field equations to external circuits and Hannalla continued to develop and simplify the coupled field and circuit model for electrical machines [62]. Today, FEM is a common tool for electric machine design, see for instance [45,51,53,63,64].

[17] http://www.vensys.de 2008-08-03

A review of coupled field and circuit problems was made by Tsukerman *et al.* in 1993 [65]. A historical review of matrix structural analysis including FEM was made by Felippa in 2001 [66].

2.5 Dynamics

Structural vibrations are an important aspect in wind turbine design. The torsional vibrations in the drive train between the turbine and the generator rotor in some cases represent the fundamental frequency of a HAWT i.e. have the lowest eigen frequency [67]. For a VAWT where the generator is placed on the ground this is an issue of even more concern since the shaft is much longer. Several studies have been made on torsional vibrations on HAWTs, see [68–74]. For VAWTs, at least two studies have been made concerning torsional vibrations and torque ripple [75, 76].

To fully understand the drive train dynamics and its interaction with the electrical system, a complete "wind to grid" model needs to be developed. An example of a model for a HAWT with a PMSG can be found in [77].

3. Theory

This chapter gives a theoretical background to the different areas presented in this thesis. The first and the second section in this chapter concern the wind resource and some basic wind turbine theory respectively. The third section deals with generator theory, where alternative ways to describe generators are discussed as well as magnetic materials, generator losses and harmonics. The fourth section covers generator modelling and describes the model used here. Finally, the fifth section covers dynamic theory and discusses torsional vibrations in the drive shaft of a wind turbine.

For derivations and further explanations of the equations and general theory presented in this section, see [16, 26, 78–84].

3.1 The wind as an energy source

The wind is an intrinsically varying energy source, which puts high demands on the technology trying to access it. The wind is varying all the time both in wind speed and wind direction. The wind speed variations can be divided into different time scales [26]. Annual variations refer to differences during one year due to different seasons. Diurnal variations cover differences during one 24 hour period, for instance the wind speed is usually higher during the day than during the night. Short-term variations refer to variations over time intervals of 10 minutes or less, normally related to turbulence or wind gusts. In addition, the wind speed varies with height, referred to as the vertical wind shear. The wind shear is usually modelled with a logarithmic profile or with a power law profile [26]. The vertical wind shear is much easier to predict over a sea surface than over land since there are no obstacles. Furthermore, the offshore wind variations are more predictable and the wind speed is usually higher than over land.

The power that can be absorbed by a wind turbine is expressed as

$$P = \frac{1}{2} C_P \rho A_t v^3 \tag{3.1}$$

where P is the absorbed power, C_P is the power coefficient (which is a function of the tip speed ratio, TSR, see section 3.2.1), ρ is the density of the air, A_t is the cross section area of the turbine and v is the wind speed. The power coefficient, C_P, states how big part of the power in the wind that is absorbed by a wind turbine. The theoretical maximum value of C_P for a HAWT is $16/27 \approx$

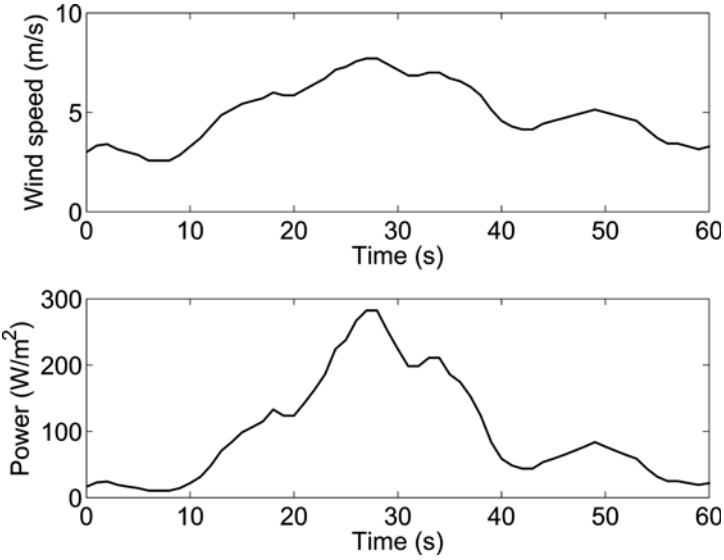

Figure 3.1: The top figure shows the wind speed variation with time. The bottom figure shows the power content in the wind.

0.59, and is called the Betz limit [85]. It has been questioned whether this limit is applicable to VAWTs [5]. The power in the wind is proportional to the wind speed cubed, as can be seen in equation (3.1), so if the wind speed is increased, the wind power is increased more. Therefore, the amount of power available for a wind turbine is highly variable. An example of the wind variations can be seen in fig. 3.1, where both the wind speed and the wind power are plotted during a short wind gust. It is clear from observing fig. 3.1 that the variations in power content are larger than the variations in wind speed.

3.1.1 Statistical wind distribution

The wind is a varying energy source and the amount of data from wind measurements is usually huge. Therefore, statistical methods are used to describe the wind. The statistical methods can be used to predict the energy potential at a site where the statistical wind distribution is known. The two distributions commonly used in wind analysis are the Rayleigh distribution and the Weibull distribution. The Rayleigh distribution is based on the mean wind speed whereas the Weibull distribution can be derived from the mean wind speed and the standard deviation and is therefore more exact but demands more information about the site. A Rayleigh distribution is a simplified Weibull distribution for which the standard deviation is 0.523 times the mean wind speed. Here, the Rayleigh distribution has been used for modelling due to its simplicity. The probability distribution function, $p(v)$,

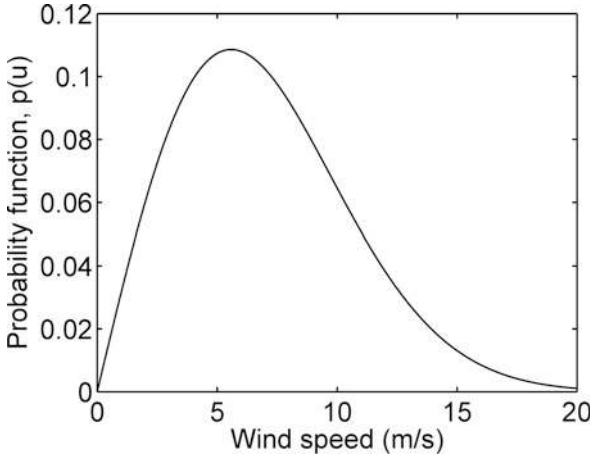

Figure 3.2: A Rayleigh distribution for a mean wind speed of 7 m/s.

for a Rayleigh distribution is

$$p(v) = \frac{\pi}{2}\frac{v}{\bar{v}^2}e^{-\frac{\pi}{4}\left(\frac{v}{\bar{v}}\right)^2} \tag{3.2}$$

where v is the wind speed and $\bar{v}$ is the mean wind speed. The probability function for a Rayleigh distribution with a mean wind speed of 7 m/s can be seen in fig. 3.2.

3.2 Wind turbine theory

3.2.1 Basic aerodynamics

The power coefficient, C_P, of eqn (3.1), is a function of the tip speed ratio, TSR, which is the ratio between the blade tip speed of the turbine and the wind speed,

$$TSR = \frac{\omega_{mech} R_0}{v} \tag{3.3}$$

where ω_{mech} is the rotational speed of the turbine, R_0 is the turbine radius and v is the wind speed. A HAWT is normally operated at a tip speed ratio of 5-7. A VAWT normally has a lower tip speed ratio. A C_P-TSR curve can be seen in fig. 3.3. The turbine should be operated at optimum tip speed ratio for maximized power absorption, as can be seen in fig. 3.3. If the tip speed ratio decreases an aerodynamic phenomena called stall will occur, where eddies will develop at the blade tip. The blade therefore absorbs less power, which explains why the C_P-TSR curve goes down. This phenomenon can be used as a power regulation strategy, see section 3.2.2.

The solidity, σ_0, is the relation between the blade area and the turbine cross section area and has different definitions for different types of turbines. For a

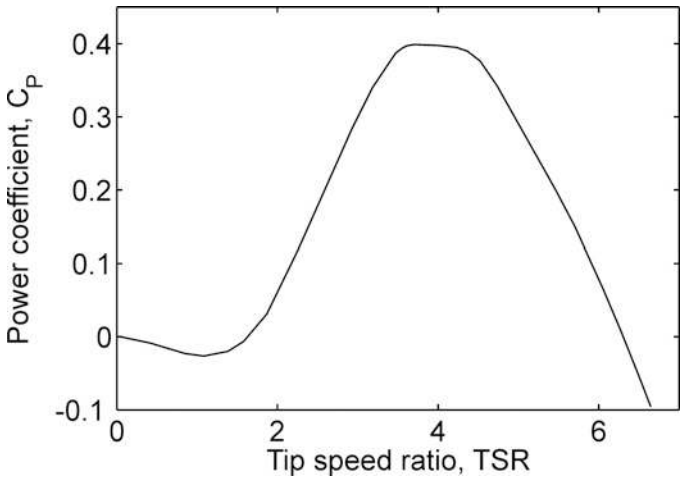

Figure 3.3: The power coefficient as a function of the tip speed ratio.

HAWT it is defined as

$$\sigma_{0,\mathrm{HAWT}} = \frac{N_B c_0}{\pi R_0} \tag{3.4}$$

where N_B is the number of blades, c_0 is the chord length, and R_0 is the radius of the turbine. For a VAWT, where each blade sweeps the cross section area twice, the solidity is defined as

$$\sigma_{0,\mathrm{VAWT}} = \frac{N_B c_0}{R_0}. \tag{3.5}$$

The VAWT considered here has a low solidity and is therefore not self-starting. This can be seen in fig. 3.3 by observing that the C_P goes down below zero for low TSR values, i.e. energy needs to be supplied for the turbine to start rotating. The start-up of a VAWT can be achieved in several ways, for instance by having pitchable blades. Another option is to have a hybrid of a straight-bladed VAWT and a Savonius turbine, since the Savonius turbine is self-starting [86]. In the concept considered here, the generator is used to electrically speed up the turbine.

The aerodynamic theory used in correlation to this work to predict the aerodynamic behaviour of the straight-bladed VAWT is an in-house made simulation tool, which is shortly explained in paper III and more deeply explained and further developed in [6].

3.2.2 Wind turbine operation and control

A wind turbine absorbs the most energy when operated at optimum TSR. However, the rotational speed of the turbine is chosen to have a maximum value. For a fixed rotational speed and with increasing wind speed, the TSR will decrease and the turbine will go into stall, which is a convenient power

control. The power is usually kept constant when the rated power has been reached and then a power control strategy has to be used to limit the absorbed power at increasing wind speeds. For most HAWTs pitch control is used, where the turbine blades are mechanically turned to absorb less power. An alternative is active stall control where the blades are mechanically turned in the opposite direction so that stall is achieved. In the concept discussed here, a strategy called passive stall control is used where a powerful generator controls the rotational speed of the turbine so that the TSR decreases and the turbine gradually stalls.

A wind turbine can be operated according to different control rules depending on the wind speed. The example shown here is taken from paper VIII, see table 3.1. Passive stall regulation is used as power control. The turbine is operated at wind speeds between 4 and 20 m/s and is rated at 12 m/s. The turbine is started when the wind speed exceeds 4 m/s. It is operated at optimum TSR, see eqn (3.3), until the wind speed exceeds 10 m/s. At wind speeds above 10 m/s the rotational speed is kept constant. The C_P will decrease slightly in wind speeds between 10 and 12 m/s. At wind speeds above 12 m/s the power will be kept constant and the wind turbine will start to stall resulting in reduced power absorption. The rotational speed might need to be reduced slightly, depending on the efficiency of the stall control. The power curve for a turbine operated according to this strategy can be seen in fig. 3.4. The rotational speed is limited not only to stall control the turbine, but also for structural reasons such as blade strength and vibrations and to limit the aerodynamic noise level. For a HAWT, operating at a higher TSR, the rotational speed limit is usually set by the allowed noise level.

Table 3.1: *The different operational modes for a 50 kW wind turbine.*

Mode	Wind speed (m/s)	Rot. speed (rpm)	Control rule
1	0-4	0	Not operated
2	4-10	26-64	Optimum TSR
3	10-12	64	Stall regulation
4	12-20	60-64	Constant power reg.
5	>20	0	Shut down

A wind turbine operated at variable speed with passive stall control will put some demands on the generator. Firstly, it is important that the generator has a high efficiency over a wide range of loads and speeds, i.e. it must have good performance at both part load operation and overload. Secondly, the generator must be strong and robust since the passive stall control means that the power is controlled electrically, by the generator controlling the rotational speed, instead of mechanically which is the usual way to control the power. The need to control the turbine at high wind speeds requires a generator with

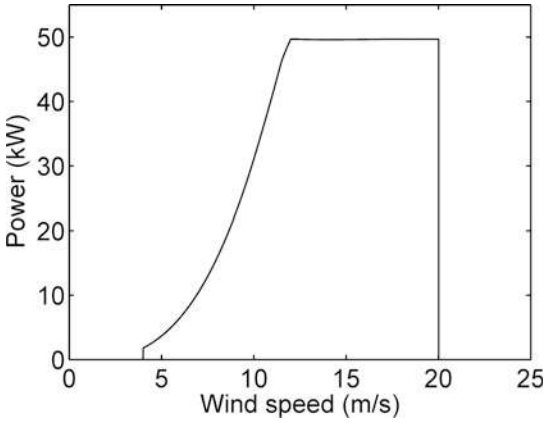

Figure 3.4: Example of a power curve for a 50 kW wind turbine following the control rules from table 3.1.

high overload capability. The overload capacity of the generator depends on the pull-out torque, which is the maximum torque that the generator can handle before becoming desynchronised. The pull-out torque is usually between 1 to 5 times the rated torque. A good measurement of the pull-out torque is the load angle at rated power, see section 3.3.5. A low load angle implies a pull-out torque several times the rated torque and thereby good overload capability. However, the overload capability is also determined by the maximum temperatures reached in the generator. The main heat source in the generator type used here are the cables [7].

3.3 Generator theory

This section presents generator theory for the generator type in focus here, i.e. a radial-flux, cable-wound, permanent magnet, direct driven synchronous generator. The section begins with an introduction to magnetic materials and their characteristics followed by a presentation of general generator theory. The following part discusses different types of losses in the generator. The fourth part discusses harmonics and armature winding. Finally, the fifth part of this section presents the circuit theory, which is a simplified way to describe a generator.

3.3.1 Magnetic materials

A permanent magnet synchronous generator has two important magnetic materials as part of its active material. These are a hard magnetic material; the permanent magnets and a soft magnetic material; the stator steel. Magnetic materials are usually described by their **B**-**H** curve, where **B** is the magnetic flux density and **H** is the magnetic field. The **B**-**H** curve describes the magneti-

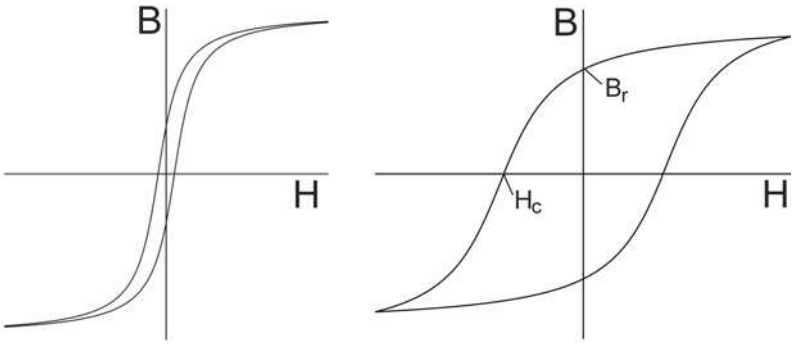

Figure 3.5: Representative **B**-**H** curves for a soft magnetic material to the left and a hard magnetic material to the right. B_r is the remanence and H_c is the coercivity.

sation process of a material. Representative **B**-**H** curves for a hard and a soft magnetic material can be seen in fig. 3.5. The permeability, μ, is a measure of how large magnetic flux density is reached in a material when a magnetic field is applied and is defined according to the equation

$$\mathbf{B} = \mu \mathbf{H} \tag{3.6}$$

A hard magnetic material is represented by high remanence, B_r, see fig. 3.5. The remanence is a measure of the remaining magnetisation when the driving field is dropped to zero. A permanent magnet holds, as its name suggests a permanent magnetisation, i.e. it has a high remanence. The magnet is magnetised in the factory and will under normal operation never be de-magnetised. The coercivity, H_c, is a measure of the reverse field needed to reduce the magnetisation to zero after a material have been saturated. Consequently, a permanent magnet should also have high coercivity. However, there can be problems with de-magnetisation in generators, if the current or temperature is too high.

A soft magnetic material has a low remanence, which means that the remaining magnetization is low when the applied field is turned off. This is a desired property for the stator steel of the generator which will be magnetised in different directions with every pole that passes by it. This means that the material travels along the line on the **B**-**H** curve, up and down, with the same frequency as the poles pass it, for instance with 50 Hz for a constant speed machine connected directly to the grid. On the contrary, a permanent magnet will under normal operation never complete one lap on the **B**-**H** curve. When a magnetic material moves one lap on the **B**-**H** curve, it is subject to a phenomenon called hysteresis, due to the non-reversible process along the **B**-**H** curve. The hysteresis yields losses in the magnetic material which are proportional to the area inside the closed **B**-**H** curve. For a soft-magnetic material, where the remanence is low, **B** and **H** are close to proportional, and the area between them can be described as a function of B^2. Hysteresis losses are discussed more in section 3.3.3.

An important property for a soft magnetic material used as stator steel in a generator is high permeability. Furthermore, a soft magnetic material should have a high magnetic saturation and low power loss. Magnetic materials can become saturated when the magnetic flux density reaches the saturation magnetic flux density. The magnetic circuit becomes inefficient when a material is saturated.

3.3.2 General theory

Generator theory is based on electromagnetism. Maxwell is the one who first explained the relationship between electric fields and magnetism in Maxwell's equations; the four fundamental equations of electromagnetism

$$\nabla \cdot \mathbf{D} = \rho_f \tag{3.7}$$

$$\nabla \cdot \mathbf{B} = 0 \tag{3.8}$$

$$\nabla \times \mathbf{E} = -\frac{\partial \mathbf{B}}{\partial t} \tag{3.9}$$

$$\nabla \times \mathbf{H} = \mathbf{J}_f + \frac{\partial \mathbf{D}}{\partial t} \tag{3.10}$$

Here, $\mathbf{D}$ denotes the electric displacement field, ρ_f is the free charge density, $\mathbf{B}$ is the magnetic flux density, $\mathbf{E}$ denotes the electric field, $\mathbf{H}$ is the magnetic field and $\mathbf{J}_f$ is the free current density. Gauss' law, eqn (3.7), expresses how electric charges produce electric fields. Eqn (3.8) shows that the net magnetic flux out of any closed surface is zero and that magnetic monopoles do not exist. Faraday's law of induction, eqn (3.9), describes how time changing magnetic fields produce electric fields. Ampere's law states how currents and changing electric fields produce magnetic fields, eqn (3.10).

The conductivity, σ, relates the free current density to the electric field according to

$$\mathbf{J}_f = \sigma \mathbf{E} \tag{3.11}$$

The principle theory explaining a generator is Faraday's law of induction, eqn (3.9), which can be rewritten as eqn (3.12) for a coil with N turns. Eqn (3.12) states that the induced (no load) voltage, E_i, in the electric machine depends on the number of turns, N, of the conductor and the time-derivative of the magnetic flux, $\partial\phi/\partial t$.

$$E_i = -N\frac{\partial \phi}{\partial t} \tag{3.12}$$

Analytical calculations on generators can be performed by using eqn (3.12) and eqn (3.14). The required generator dimensions for a certain voltage level can be found using eqn (3.12) by assuming an effective value of the magnetic flux density in the stator teeth and by making appropriate design choices for a few variables. However, losses are not included in this calculation, so the resulting generator dimensions will be slightly smaller than what is realistic.

The magnetic energy, W_E, in a volume, τ, is defined as

$$W_E = \frac{1}{2} \iiint_{\tau} \mathbf{H} \cdot \mathbf{B} d\tau \tag{3.13}$$

In a generator, the magnetic energy is dominated by the energy in the airgap and in the PMs as the permeability for the other materials in the magnetic circuit is very high. Thus, the magnetic energy in the airgap can be written as

$$W_E \approx \frac{B_{eff}^2}{2\mu} s A_{airgap} \tag{3.14}$$

where B_{eff} is the effective magnetic flux density in the airgap, μ is the permeability in the airgap, s is the airgap length and A_{airgap} is the cross section area of the airgap.

The required dimensions of the generator in order to achieve the desired power level, can be found by using eqn (3.14) and by making assumptions of the values of the load angle (see section 3.3.5), the effective value of the magnetic flux density in the airgap and the rotational speed.

When a current is run in the armature of a generator a magnetic field opposing the field from the magnets is induced. This field, the armature reaction, increases with increasing current and causes a voltage drop in the armature voltage. The voltage drop depends on the machine reactance, see section 3.3.5. It is therefore desired to design generators with low machine reactance. A generator designed with a low load angle will have a small voltage drop at rated operation.

3.3.3 Generator losses

Generators suffer from electromagnetic and mechanical losses. The electromagnetic losses consist of losses in the copper conductor and iron losses. The latter are divided into hysteresis losses, eddy current losses, excess (or anomalous) losses and rotational losses. The mechanical losses are, in the absence of a gearbox, dominated by losses in couplings and bearings. Furthermore, windage losses in the generator are usually included in the mechanical losses.

The iron losses in the stator can be represented by the expressions following below [87, 88]. The iron losses are caused by complicated magnetic phenomena and the formulas presented below are based on empirical studies. The losses are given in W/m^3 and have to be multiplied with the volume to find the total losses in W.

As was discussed in section 3.3.1, hysteresis describes the phenomenon that a physical process does not follow the same path when its direction is reversed. The area enclosed by the **B**-**H** curve represents the hysteresis losses, P_{loss}^{hy}, which are a function of B^2 and the electric frequency, f, and usually are expressed as

$$P_{loss}^{hy} = k_f k_h B_{max}^2 f \tag{3.15}$$

where B_{max} is the maximum magnetic flux density, f is the electrical frequency, k_f is the stacking factor and k_h is the hysteresis loss coefficient. The stacking factor is a non-dimensional factor indicating how much of the stator volume that is filled up with stator steel. Usually, the product of the number of steel plates and the thickness of each plate is smaller than the height of the stator.

Eddy currents are induced by changing magnetic fields in conducting material. The eddy current losses are efficiently minimized by having a laminated stator steel core. The eddy current losses, P_{loss}^{ed}, can be written as

$$P_{loss}^{ed} = k_f k_{eddy} (B_{max} f)^2 \tag{3.16}$$

where k_{eddy} is the eddy current loss coefficient and is defined as

$$k_{eddy} = \pi^2 \frac{\sigma d^2}{6} \tag{3.17}$$

where σ is the conductivity and d is the sheet thickness of the stator steel.

The calculated values of hysteresis losses and eddy current losses will differ slightly from measured values. The difference is attributed to the excess losses if rotational losses can be omitted [89,90]. The excess losses, P_{loss}^{ex}, depend on domain-wall motion as the domain structure changes when a magnetic field is applied and are described as

$$P_{loss}^{ex} = k_f k_e (B_{max} f)^{1.5} \tag{3.18}$$

where k_e is the excess loss coefficient.

The rotational iron losses are a result from the rotating **B** vector. No rotational losses occur if a **B** vector alternating with 180 degrees can be assumed. However, if the **B** vector in the steel is rotating less than 180 degrees, losses will occur [91, 92]. For a well designed generator the rotational losses can be minimized to only constitute a few per cent of the iron losses. The place in a generator that usually has highest rotational losses is the tooth root region in the stator yoke [92, 93].

Parts of the stator steel with a high **B** value will have large power loss. The power loss yields heat and these parts can become hot spots, which need to be cooled or, preferably, avoided.

The total iron losses, P_{loss}^{Fe}, are

$$P_{loss}^{Fe} = (P_{loss}^{hy} + P_{loss}^{ed} + P_{loss}^{ex} + P_{loss}^{rot}) V_s \tag{3.19}$$

where V_s is the stator steel volume and P_{loss}^{rot} denotes the rotational losses.

The losses in the conductors of a generator consist of resistive losses and eddy current losses. The eddy current losses in the copper windings are usually small. The losses in the conductors of a three-phase generator, P_{loss}^{Cu}, can be written as

$$P_{loss}^{Cu} = 3 R_i I^2 + P_{loss}^{Cu,ed} \tag{3.20}$$

where R_i is the inner resistance in the cable, I is the current and $P_{loss}^{Cu,ed}$ denotes the eddy current losses in the cables. The inner resistance, R_i, is defined as

$$R_i = \frac{l}{\sigma A_{Cu}} \tag{3.21}$$

where l is the cable length and A_{Cu} is the conductor area. The conductors are usually stranded due to the skin effect. According to the skin effect there will be an accumulation of electrons at the surface of a conductor, which can lead to higher resistance than expected and less effective use of the conductor if the conductor thickness is too large. The skin depth is defined as the distance during which the current density has declined to 1/e of its value at the surface[1]. The frequency dependent skin depth, δ_s, is defined as

$$\delta_s = \frac{1}{\sqrt{\pi f \mu \sigma}} \tag{3.22}$$

The eddy current losses are decreased in stranded conductors. Another reason for the low amount of eddy current losses in the copper conductors is the low permeability of copper.

The eddy current losses in the PMs and in the iron ring that the PMs are mounted on can usually be neglected. The magnetic flux density in the PMs and in the iron ring is not time-changing but rather constant and does not induce eddy currents. However, there is a small time-dependent part of the magnetic flux density in the rotor resulting from harmonics but it is usually omitted [94].

The total electromagnetic losses, P_{loss}, are found from

$$P_{loss} = P_{loss}^{Cu} + P_{loss}^{Fe}. \tag{3.23}$$

The electric efficiency, η_{el}, of the generator is determined by finding the losses of the generator and becomes

$$\eta_{el} = \frac{P_{el}}{P_{el} + P_{loss}}. \tag{3.24}$$

where P_{el} is the electric power.

The resistive losses can be determined by measuring the current and the inner resistance in the cables. The losses in the stator steel can be determined by measuring the no load torque, which also includes mechanical losses.

3.3.4 Harmonics and armature winding

The voltage from a generator may contain harmonics. Harmonics are parts of a signal that have frequencies that are integer multiples of the fundamental

[1] $e = 2.718...$ and $1/e \approx 0.37$

frequency. Harmonics can cause problems on the grid, for instance by disturbing electric equipment and can induce large frequency dependent losses. Furthermore, harmonics have negative effects on the generator such as increased losses and pulsating torques [95]. Therefore, it is important to analyse the harmonic content of the generator voltage. The voltage can be divided into its different components i.e. the sinus-curves of each harmonic as shown in eqn (3.25).

$$U(t) = U_1 \sin(\omega_{el} t) + U_2 \sin(2\omega_{el} t) + U_3 \sin(3\omega_{el} t) + ... \tag{3.25}$$

where $U(t)$ is the total voltage signal, ω_{el} is the fundamental frequency and U_i ($i = 1, 2, 3...$) is the amplitude of each harmonic. Normally, only odd harmonics are present in the terminal voltage of the generator due to half-wave symmetry. The 3^{rd} harmonic is present in the phase voltage but will be suppressed in the line voltage for a three phase system. The voltage harmonic content can be decomposed through Fourier analysis of the voltage signal.

The harmonics originate from the shape of the magnetic flux density in the airgap, which is affected by the geometry of the stator. Harmonics will always be present to some extent, since the windings are embedded in slots which can not be perfectly sinusoidally distributed. Furthermore, the magnet geometry can also affect the shape of the output.

Harmonics can be reduced by incorporating distributed windings and fractional pitch windings. However, apart from reducing the harmonics, this also causes a small decrease in the fundamental tone of the voltage. Distributed windings means that the windings of all phases are distributed throughout the entire circumference of the generator, as opposed to concentrated windings where the windings for each phase are concentrated. Fractional pitch windings means that the number of slots per pole and phase differs from one. The number of slots per pole and phase can be chosen so that the result is a complete suppression of a chosen harmonic. [95]

A number of slots per pole and phase of one, will give ripple in the torque due to the attracting forces between each magnetic pole on the rotor and an electric pole on the stator. The ripple has the same frequency as the electrical frequency and is usually called cogging. The cogging can be reduced substantially by choosing a number of slots per pole and phase different from one.

3.3.5 The circuit theory

The synchronous generator can be represented by an equivalent circuit and a phasor diagram, see fig. 3.6. The equivalent circuit has the equation

$$\hat{E}_i = \hat{U} + \hat{I}R_i + \mathrm{j}\hat{I}X_d \tag{3.26}$$

where $\hat{}$ denotes phasors and E_i is the no load voltage, U is the terminal voltage, I is the output current, R_i is the inner resistance and X_d is the machine

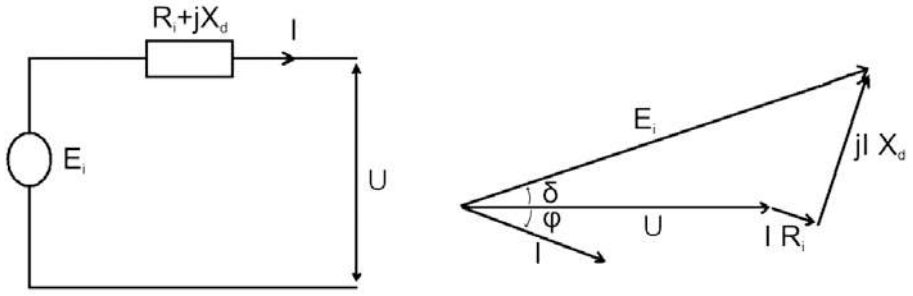

Figure 3.6: The equivalent circuit and the phasor diagram for a synchronous generator.

reactance. By writing out the complex numbers, eqn (3.26) is written as

$$E_i(\cos\delta + \mathrm{j}\sin\delta) = U + (R_i + \mathrm{j}X_d)I(\cos\varphi - \mathrm{j}\sin\varphi). \tag{3.27}$$

The power factor angle, φ, is the phase angle between the voltage and the current. If the generator is connected to a purely resistive load the power factor angle measured over the electrical load is zero. The load angle, δ, is the phase angle between the no load voltage and the load voltage. It represents the small tilt of the magnetic field lines in the airgap due to the loading of the generator, i.e. the angle between the rotor and the resultant field.

The power output from the generator is found from

$$\hat{S} = \hat{U}\hat{I}^* = |U||I|(\cos\varphi + \mathrm{j}\sin\varphi) = P_{el} + \mathrm{j}Q \tag{3.28}$$

where $\hat{S}$ is the apparent power, P_{el} is the electric power and Q is the reactive power. The factor, $\cos\varphi$, is called the power factor.

3.4 Electromagnetic modelling

The electromagnetic model used here is described by a combined field and circuit equation model, which is a common approach to solve electromagnetic problems in electric machine design [96]. The magnetic field inside the generator, assumed to be axi-symmetrical, is modelled in two dimensions. The field model describing the generator is based on Maxwell's equations, eqn (3.7)-(3.10). Here, the time derivative of the electric displacement field, $\partial\mathbf{D}/\partial t$, can be neglected due to the low frequencies. For the stationary condition the electric field, $\mathbf{E}$, can be written as

$$\mathbf{E} = -\nabla V \tag{3.29}$$

where V is the electric potential.

The magnetic flux density, $\mathbf{B}$, can be written in terms of a magnetic vector potential, $\mathbf{A}$, according to

$$\mathbf{B} = \nabla \times \mathbf{A} \tag{3.30}$$

By combining Maxwell's equations with the relations from eqn (3.6), (3.11), (3.29) and (3.30), the field equation is found [62]

$$\sigma \frac{\partial A_z}{\partial t} - \nabla \cdot \left(\frac{1}{\mu} \nabla A_z \right) = -\sigma \frac{\partial V}{\partial z} \tag{3.31}$$

where A_z is the axial magnetic potential, μ is the permeability, σ is the conductivity and $\partial V / \partial z$ is the applied potential. The field equation will give a solution for the magnetic vector potential A_z and thereby gives the magnetic flux density, **B**. The term $\sigma \frac{\partial A_z}{\partial t}$, which usually is small, represents the induced eddy currents in the conductors and depends on the skin depth, see eqn (3.22). The right-hand term in eqn (3.31) represents the applied currents in the $\hat{z}$-direction and can be rewritten as [62]

$$-\sigma \frac{\partial V}{\partial z} = J_0 + J_{pm} \tag{3.32}$$

where J_0 is the current density in the conductors and J_{pm} is the current density that represents the permanent magnets and is described in the next section.

Circuit equations represent the stator. Three-dimensional effects such as end region fields are taken into account by coil end impedances in the circuit equations of the windings. The circuit equations are defined as

$$I_a + I_b + I_c = 0 \tag{3.33}$$

$$U_{ab} = U_a + R_i I_a + L_s^{end} \frac{\partial I_a}{\partial t} - U_b - R_i I_b - L_s^{end} \frac{\partial I_b}{\partial t} \tag{3.34}$$

$$U_{cb} = U_c + R_i I_c + L_s^{end} \frac{\partial I_c}{\partial t} - U_b - R_i I_b - L_s^{end} \frac{\partial I_b}{\partial t} \tag{3.35}$$

where a, b and c denotes the three phases, I_a, I_b, I_c are the conductor currents, U_{ab} and U_{cb} are the terminal line voltages, U_a, U_b, U_c are the terminal phase voltages, R_i is the inner resistance and L_s^{end} is the coil end inductance. For a pure resistive, Y-connected load the external circuit equations are

$$U_{ab} = R_L I_a - R_L I_b \tag{3.36}$$

$$U_{cb} = R_L I_c - R_L I_b \tag{3.37}$$

where R_L is the load resistance.

3.4.1 Permanent magnet and stator steel modelling

The permanent magnets are modelled according to the current sheet approach [97, 98], where the PM is modelled as a current carrying coil with the same dimensions as the PM. The magnet is modelled with a current sheet on its

surfaces. The current sheet should be oriented so that it magnetizes the material in the same direction as the magnetization of the original magnet. The magnetising current is decided by the equation

$$I_{pm} = H_c h_{pm} \tag{3.38}$$

where, I_{pm} is the coil current representing the magnet, H_c is the coercivity and h_{pm} is the height of the PM. However, the magnetisation profile for the PM used in the model has to be shifted so that the curve passes through origin, to be valid. When the curve is shifted, the value of H_c will equal B_r/μ so that the current becomes

$$I_{pm} = \frac{B_r h_{pm}}{\mu} \tag{3.39}$$

where B_r is the remanence. The current density J_{pm} used in eqn (3.32) is found from the current I_{pm}.

The nonlinear behaviour of the laminated stator steel, as exemplified in fig. 3.5, requires a nonlinear representation. The **B**-**H** curve is modelled as a nonlinear, single-valued curve and the hysteresis effect is thereby neglected [99]. However, the hysteresis losses are taken into account according to the procedure explained in section 3.4.2 by using the equations from section 3.3.3.

3.4.2 Loss modelling

The electromagnetic losses are modelled by using the equations described in section 3.3.3. The copper losses are easier to simulate than the iron losses. For the iron losses, data from the steel manufacturer for a couple of frequencies (usually 50, 100 and/or 200 Hz) is used to estimate the loss distribution between the different types of losses and to interpolate the results for all different frequencies. In the data from the manufacturer the rotational losses are not present, since the steel has been tested with a **B** vector alternating with exactly 180 degrees. There are several ways to model the rotational losses. The method used here is described in [100].

In the simulations a loss correction factor of 1.5 is used for all iron losses, i.e. the total iron losses are multiplied by 1.5. The loss correction factor represents differences in the theoretical modelling of iron losses and experimental measurements [88]. The choice of a loss correction factor of 1.5 is taken from the experimental verification of the simulation method using measurements on several large generators used for hydropower.

Possible reasons for the problems with the theoretical model of the iron losses are:
1. Only the maximum magnetic flux density, B_{max}, is used in the modelling, i.e. **B** is modelled as a perfect sinusoidal waveform, which it is not, i.e. the harmonics of **B** are not included in the modelling.
2. The steel might have other properties than stated by the manufacturer.

3. The characteristics of the steel can change during laser cutting and preparation.
4. A two-dimensional model is used to model a three-dimensional generator, i.e. end effects are omitted. The iron losses might be higher than expected at the ends.

3.5 Dynamic theory

3.5.1 Torsional vibrations

Many fractures in machines and other mechanical structures originate from vibrations. If an external torque affects the vibrations of a structure the system is subject to forced vibrations. The equation of motion for a damped system subject to a time-dependent torque, $M(t)$, is.

$$M(t) - k_0\theta - c\frac{d\theta}{dt} = J_m\frac{d^2\theta}{dt^2} \tag{3.40}$$

where θ is the angular displacement, k_0 denotes the rotational stiffness, c is the damping constant and J_m is the mass moment of inertia of the object. The time-dependent torque, $M(t)$, can be written as

$$M(t) = M_0 \sin(\omega t) \tag{3.41}$$

where M_0 is the amplitude and ω is the angular frequency. Eqn (3.40) has the solution

$$\theta(t) = \frac{M_0}{k_0}\frac{\sin(\omega t - \gamma)}{\sqrt{[1-(\omega/\omega_n)^2]^2 + [2\xi(\omega/\omega_n)]^2}} \tag{3.42}$$

where ω_n is the eigen frequency of the vibrations, γ is a phase angle and ξ is the non-dimensional damping ratio described as

$$\xi = \frac{c}{2J_m\omega_n} \tag{3.43}$$

From eqn (3.42), a dimensionless amplitude can be derived, as in eqn (3.44).

$$\frac{\theta k_0}{M_0} = \frac{1}{\sqrt{[1-(\omega/\omega_n)^2]^2 + [2\xi(\omega/\omega_n)]^2}} \tag{3.44}$$

This dimensionless amplitude can be plotted against a dimensionless frequency, to study the damping of the vibrations caused by the applied torque, see fig. 3.7. When the frequency of the applied torque equals the eigen frequency of the vibrations, i.e. when $\omega = \omega_n$, a phenomenon called resonance is reached and the amplitude in fig. 3.7 increases suddenly. This increase implies an increase in the angular displacement of the object, which might cause a fracture or in a longer time-frame fatigue. The increase

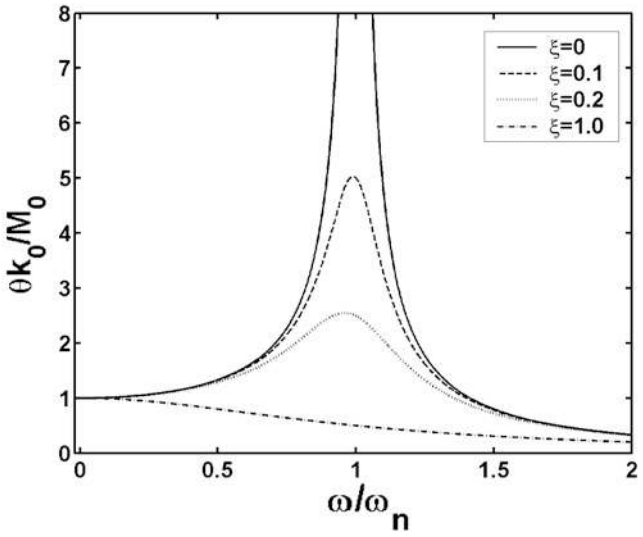

Figure 3.7: Dimensionless amplitude versus dimensionless frequency for different values of the non-dimensional damping ratio ξ. When ξ is zero, the dimensionless amplitude goes to infinity at ω/ω_n=1.

in amplitude depends on the non-dimensional damping ratio, ξ, which represents the damping of the system. If a system has sufficient damping, resonance is less dangerous for the system survival. However, resonance is not always a phenomenon that is avoided. In some applications it is desired to reach resonance.

The eigen frequency, ω_n, of the torsional vibrations can be approximated by

$$\omega_n = \sqrt{\frac{k_0}{J_m}}. \tag{3.45}$$

For the damped vibration considered here, the eigen frequency actually becomes

$$\omega_d = \sqrt{1-\xi^2}\omega_n. \tag{3.46}$$

However, since the term $\sqrt{1-\xi^2}$ usually is very close to one, it can be neglected and eqn (3.45) is valid.

The drive shaft of a wind turbine has to be constructed to avoid resonant vibrations, so that the smallest eigen frequency of the torsional vibrations, ω_n, is larger than the angular frequency of the applied torque, ω. The mass moment of inertia of the shaft can be neglected, since it is much smaller than the mass moments of inertia of the two oscillating masses. The torsional vibrations concerned here can be described by eqn (3.40). For a vertical axis wind turbine shaft the triggering torque usually has the frequency of ω_{mech}, $N_B\omega_{mech}$ or $2N_B\omega_{mech}$, where ω_{mech} is the rotational frequency of the turbine and N_B is the number of blades. $N_B\omega_{mech}$ represents the large torque oscillation due to

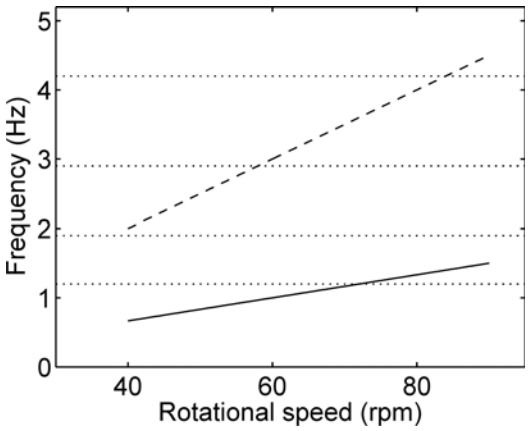

Figure 3.8: Campbell diagram. The solid line represents the rotational speed (ω_{mech}), the dashed line represents three times the rotational speed ($N_B\omega_{mech}$ for $N_B = 3$) and the dotted lines represent possible excitation frequencies.

the alternating angle of attack on the turbine blades and $2N_B\omega_{mech}$ originates from that the torque for each blade oscillates twice per revolution, where the upwind torque is larger than the downwind torque.

In order to find points of correspondence between eigen frequencies, ω_n, and possible excitation frequencies, ω, a Campbell diagram can be drawn, see fig. 3.8. In a Campbell diagram critical speeds can be found, i.e. rotational speeds for which the lines coincide. Critical speeds might be avoided by quickly speeding the turbine past these speeds. The acceptable value of the ratio ω/ω_n, without the risk of failure, depends on the generator damping, see fig. 3.7.

A conventional generator will be connected to the turbine shaft through a gearbox, since the rotational speed has to be increased for the generator to work properly. For geared systems, the inertias can be referred to their equivalent values on a single shaft. If the speed ratio between the two shafts is n, the equivalent value of the inertia, $J_{m,eq}$, will be n^2 times the inertia of the generator. This can be expressed as

$$J_{m,eq} = n^2 J_m. \tag{3.47}$$

Thus, the use of a gearbox will have a great impact on the mass moment of inertia connected to the rotor shaft, as is shown in paper II. According to eqn (3.45), a larger mass moment of inertia results in a lower eigen frequency.

The model used here based on eqn (3.40) is a one-mass model, where the mass of the turbine and the generator are lumped into one single rotating mass. However, a more precise model would be to use a two-mass model [73, 74]. The shaft can be modelled as a torsional spring between two oscillating masses, the turbine and the generator. The two types of models are compared with experimental data in [74] and the one-mass model is shown to be limited in giving correct results and in modelling the situation correctly.

4. Method

The work presented in this thesis is based on both simulations and experiments. This chapter presents the simulation method and experimental setups used in this work. The first part describes the simulation method, which is based on the model discussed in the previous chapter. The second part describes the design procedure by presenting the methodology used to design the 12 kW generator. The first part in the section on experiments presents the generator experimental setup and experiments in the laboratory and the last part of this chapter presents the VAWT setup and the experiments on the complete wind turbine.

4.1 Simulations

4.1.1 Simulation method

When simulating a generator, the electromagnetic model presented in section 3.4 is solved in the finite element environment ACE [101] by using the method[1] described here. The simulation method has been experimentally verified by using measurements from several large 50 Hz hydropower generators. Simulations can be performed either in the stationary mode where the results are given for a fixed rotor position or in a dynamic mode including the time-dependence and thereby giving more accurate results.

Geometry and material properties

The geometry of the two-dimensional cross section in which the problem is solved is specified before the simulations begin. However, the height of the generator is one of the resulting parameters from the simulations and is set by the desired, specified voltage that should be obtained. All other geometrical parts are specified and separated from each other since they will have different material properties such as conductivity, permeability, density, sheet thickness etc. A sketch showing an example of a geometry and the different materials, indicated by different colours, is shown in fig. 4.1.

The finite element method

The finite element method (FEM) is based on that the geometry is divided into small triangular parts, where the sets of equations are solved in each element.

[1] Arne Wolfbrandt and Karl-Erik Karlsson are acknowledged for doing the programming.

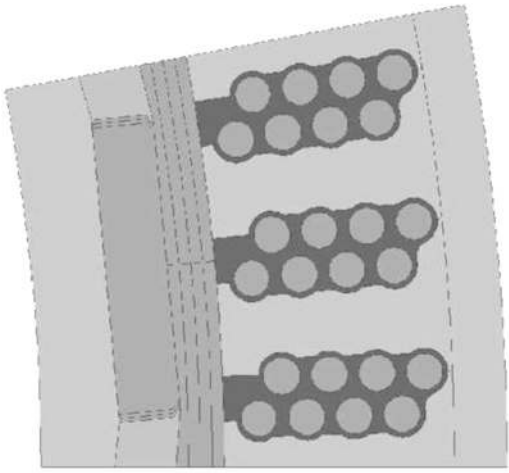

Figure 4.1: Example of a simulated geometry. The different materials are indicated by different colours.

Here, the set of equations presented in section 3.4 is solved with FEM for the generator geometry discussed above. A mesh is generated based on the chosen accuracy, see fig. 4.2. The mesh is finer close to critical parts such as airgap and cables and coarser in areas like the yoke of the stator. The possibility to increase the precision in more important parts of the geometry is one of the benefits with FEM. The problem can be solved using FEM after the geometry has been set and a mesh has been generated, dividing the geometry into small elements.

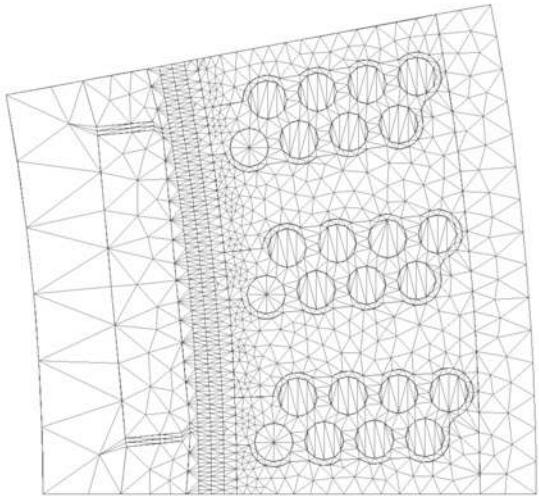

Figure 4.2: Example of mesh for one pole.

Suitable interpolation polynomials, called shape (or basis) functions are used to approximate the unknown function within each element [60]. Different degrees of the shape functions can be used. The accuracy of the calculations depends on the shape function used, linear with 3 nodes (one node in each corner of the triangle), quadratic with 6 nodes (corner nodes and mid-side nodes) or cubic with 10 nodes (corner nodes, nodes on the sides and in the middle of the triangle). Polynomials of higher orders generate better approximations of the exact solution but require longer computational time.

Boundary conditions

One of the benefits with using the finite element method for simulating a generator is that the computational time can be decreased substantially by using the symmetry of the generator. Only one pole has to be modelled if the number of slots per pole and phase is one. If it is larger than one, usually only a few poles have to be modelled to simulate the complete generator. The cell that is modelled have the boundary conditions of the vector potential set to zero at the outside of the stator and at the inside of the rotor ring, see fig. 4.3. Cyclic boundary conditions for the magnetic vector potential on the adjacent sides of the cell are required. The absolute values of the boundary conditions have to be equal and differ in sign depending on the number of poles modelled (fig. 4.3).

When a dynamic simulation is performed, the dynamic behaviour would demand a remeshing of the mesh each time the rotor moves one step. However, this can be avoided by using a moving boundary technique. The stator has a different coordinate system than the moving rotor. The boundary condition for

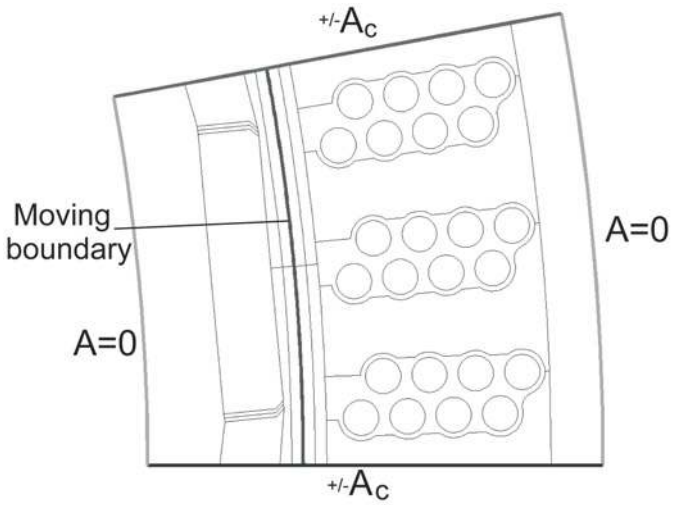

Figure 4.3: Boundary conditions for a cell with one pole, where A is the magnetic vector potential and A_c is the cyclic boundary condition for the magnetic vector potential.

the middle of the airgap (fig. 4.3) is set at the same value for the stator and the rotor. For each time-step this value is kept identical in both geometries. In this way the whole mesh does not have to be reconstructed for every time step.

Design procedure

When a generator is designed using the simulation method described here, a problem with many degrees of freedom has to be handled. In order to model the generator and find the design parameters, a number of parameters have to be decided initially. For instance, at the start of a simulation, values for the desired power level, voltage level and some geometrical constraints have to be preset. The length of the generator required to achieve the desired voltage level is a result from the simulations. The fixed parameters can be varied between different simulations. Results from a dynamic simulation of a generator, can be seen in fig. 4.4, where the magnetic flux density is shown for one pole.

When optimising the design of a generator, several simulations need to be performed. Different designs are tested through an iterative process. Thus, the design procedure is based on several simulations. In order to find a satisfying design, it is preferable to concentrate the design process on changing one parameter at a time and on optimising a few specific parameters.

The dynamic (time-stepping) simulations take far longer time than the stationary simulations. It has therefore been incorporated to use stationary simulations for designing generators when plenty of computations have to be performed through the iterative design process. The geometry is always found from performing a stationary simulation. For a fixed geometry, the dynamic model is used to achieve more accurate solutions and to simulate different situations, for instance to perform tests at part load and overload.

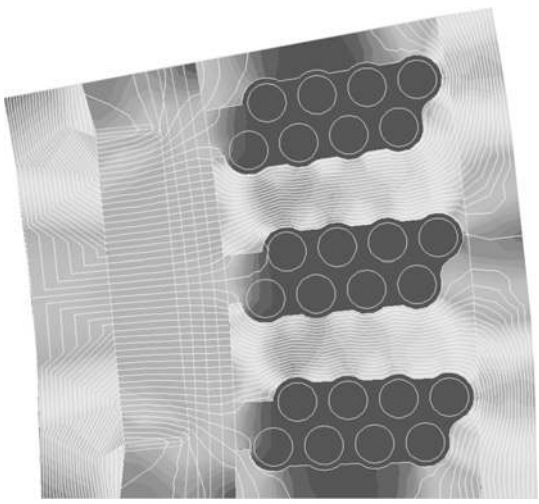

Figure 4.4: Magnetic flux density with field lines shown for one pole. Lighter areas indicate a higher magnetic flux density and darker areas indicate a lower flux density.

4.1.2 Design of the experimental generator

In this section, the design process used when the 12 kW direct driven PM synchronous generator was designed is presented and several of the design choices are motivated and explained. However, since the design process was to solve a multi-variable problem, a different approach could have been used. An example of the layout of the generator can be seen in fig 1.3.

The turbine of the VAWT was designed to absorb 12 kW at a rotational speed of 127 rpm and a wind speed of 12 m/s. The simulation method described in section 4.1.1 was used to design a generator suitable for this turbine. The resulting generator characteristics can be seen in table 4.1.

The designed turbine set the power level and the rotational speed of the generator. The first considerations were mechanical, electrical or material limitations on the design. Here, it was decided to use 16 mm^2 cable, partly since this cable was in the right regime for a 12 kW design and partly since the cable had already been tested in a previous generator constructed in the laboratory. The generator design was not optimised on lowering the generator weight or cost, rather to have an efficient generator that would be straightforward to construct. Therefore, a relatively wide airgap of 10 mm was chosen in order to simplify the mechanical construction of the generator. A wide airgap reduces the flux density and therefore larger magnets are required. The choice of current density set the voltage level, since the cable size was already decided. A current density of 1.6 A/mm^2 was chosen after thermal considerations concerning the desired overload capability. It was desired to overload the generator in current up to 30 kW, i.e. having a current density of, at least, 2.5 times the rated cur-

Table 4.1: *Generator characteristics from stationary simulations.*

Rated power (kW)	12.0
Phase voltage (V) rms	156
No load phase voltage (V) rms	161
Current (A) rms	25.7
Electrical frequency (Hz)	33.9
Electrical load (Ω)	6.08
Load angle (°)	5.3
Efficiency (%)	95.9
Rotational speed (rpm)	127
Number of poles	32
Number of slots per pole and phase	5/4
Stator inner diameter (mm)	760
Stator outer diameter (mm)	859/886
Airgap width (mm)	10
Generator length (mm)	222

rent density (compensating for the voltage drop due to the increased armature reaction), which was expected to be acceptable after considering thermal investigations already made [7]. The current was thereby set to 25.7 A and the phase voltage to 156 V.

The simulation method was then used to find an appropriate design. Designing a generator is an iterative problem with several degrees of freedom. The design objective was to find a good magnetic circuit in the generator where all magnetic materials were used properly and to avoid areas with too high magnetic flux density, which could lead to magnetic saturation. The target was to achieve suitable values for the magnetic flux density in the airgap, stator teeth and the yoke.

Two rows of cables per slot were used instead of one. The magnetic properties would be similar for both designs. The choice of two rows of cables per slot might lead to heat pockets between the cables that would be difficult to model and thereby predict. However, two rows of cables might simplify the winding of the generator and would be cheaper to laser cut. The choice of using two rows of cables was taken mostly from a research point of view since other generators under construction at the division had one row per slot. A design of four cables per row was set after evaluating different options and finding that the choice of four cables per row gave the best performance and not too long teeth, which might give structural problems.

The inner stator diameter was set to 760 mm. This was also a compromise between different features. A large diameter gives a good magnetic circuit and a low weight since the airgap velocity then is high. However, the frequency increases, which leads to more frequency dependent iron losses when the diameter is increased. A generator with a large diameter requires a more complicated support structure which might increase the weight substantially. Furthermore, a large diameter might increase the costs for manufacturing, transportation and generator housing. The number of slots per pole and phase was chosen to be close to one, mainly for constructional issues, since a reasonable size of PMs was desired. A number of slots per pole and phase of 5/4 was chosen to reduce cogging, which is usually high if one slot per pole and phase is used and since this fitted well in with the planned design. The electrical frequency was set to 33.9 Hz. The number of poles on the rotor was then set to 32.

The magnet dimensions were also investigated thoroughly. Through simulations it was found that the magnets should be as wide as possible without having too much leakage flux. From the diameter and the number of poles the pole width was found. The magnet width was set to 54 mm, covering 74% of the pole width. The height of the magnet was chosen to be 14 mm after careful consideration. When the magnet height is increased, the generator becomes more compact; the length decreases and the load angle decreases. However, the iron losses increase since more stator yoke is needed and the PM weight increases. The PMs constitute the largest cost in a mass produced machine. However, in a one-off machine the laser cutting of the stator steel is more ex-

pensive. For this generator, the total mass was minimized when the magnet height was set to 16mm. The PM weight decreased when the magnetic height was decreased. However, the total rotor weight was minimized for a magnet height of 12 mm, which is important when shaft vibrations are concerned. A height of 14 mm was chosen as a compromise between reducing the weights and thereby considering the costs.

The stator steel has a thickness of 0.5 mm, chosen as a compromise between the increased cost of laser cutting more steel and the eddy current losses that increase quadratically with increasing thickness. The chosen steel is M270_50A[2], which has rather good loss characteristics. The magnets are made of Neodymium-Iron-Boron of the type N40[3]. The magnets are slightly curved and are mounted on an iron ring. The thickness of the iron ring was chosen so no magnetic saturation would occur. The magnets are separated and fixed by Aluminium wedges (see fig. 4.6).

The cables are of the type MK16[4], which have a cross section area of 16 mm^2, have PVC insulation and are stranded. The order of the three phase stator windings was derived by the established 5/4 slots per pole and phase. A winding scheme was found by trying to limit the cable in the end windings. An auxiliary winding was introduced in the back of the stator slot. The auxiliary winding was to be used for starting the wind turbine, since the turbine is not self-starting. It was also wound with MK16 cable and is electrically insulated from the main winding.

The outer diameter of the generator was set to 859 mm in the design process. However, in the final design of the generator an extra winding hole for the auxiliary winding was introduced. Furthermore, bolt holes and holes for wedges were needed. Therefore, the outer diameter was extended to 886 mm. In the simulations the auxiliary winding and the holes for bolts and wedges are omitted. An outer diameter of 875 mm was used for the simulations, since the simulated stator area then is the same as for the constructed stator steel.

4.2 Experiments

4.2.1 Generator experimental setup and experiments

The generator was constructed according to the design presented in section 4.1.2. In addition, the design was completed with supporting material consisting of an interior rotor including the drive shaft, as well as beams, a top plate and a bottom plate for the stator. The construction of the generator is covered more in paper IV. The purpose of having an experimental setup with a generator was to calibrate simulations and to demonstrate the technology.

[2]http://www.sura.se 2008-07-17

[3]http://www.suramagnets.se/pdf/suramagnets_sintered_nd-fe-b.pdf 2008-07-17

[4]http://www.draka.se/Portals/0/Produkter/Pdf/MK_450750_V.pdf 2008-07-17

The generator was tested in the laboratory before being mounted in a 12 kW VAWT, see fig. 4.5. A close-up view of the airgap can be seen in fig. 4.6. A second experimental generator setup, identical to the first one, was recently finished in the laboratory.

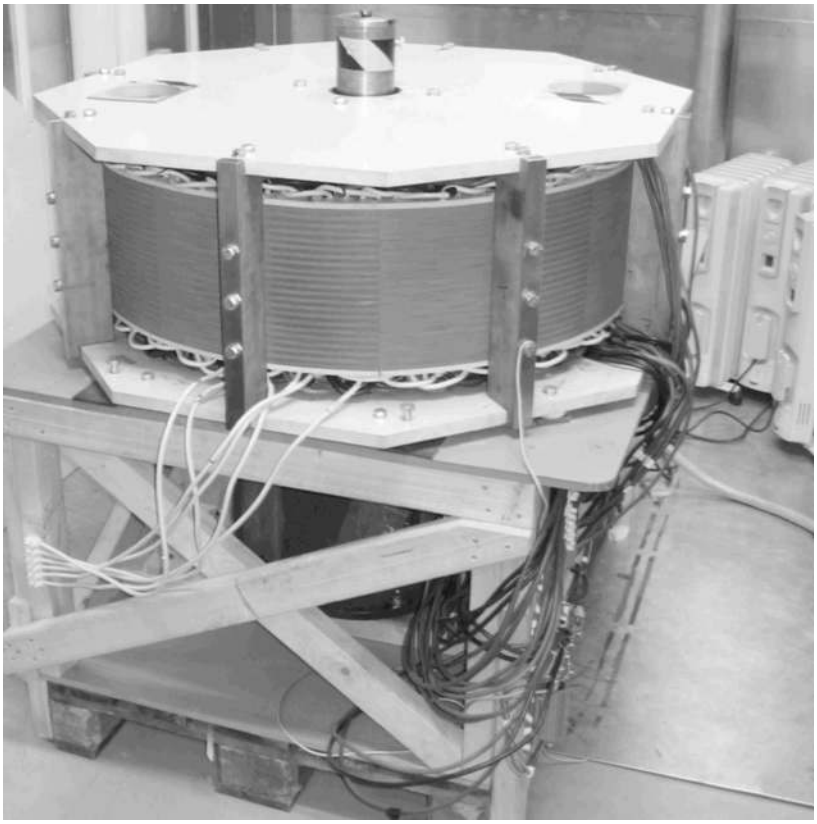

Figure 4.5: The first experimental generator.

The first and the second experimental setups are identical and consist of an electric motor, a gearbox, a frequency converter, the 12 kW generator and an electrical load, see fig. 4.7. An asynchronous 30 kW, 1500 rpm motor[5] is used together with the frequency converter[6] to run the generator at variable speed. A right angle spur gear[7] is connected between the motor and the generator due to their different rotational speeds. The generator is connected to an electrical load. The whole experimental setup is mounted on a support structure, which was made of wood for the first setup and is made of steel for the second setup.

[5] A squirrel cage aluminium motor of type M2AA 200 L from ABB.
[6] A standard frequency converter from ABB of type ACS550-01-072A-4.
[7] Type IB123 from Motovario.

Oscilloscopes[8] and probes[9] are used to measure the voltages and currents[10] for all phases. The generator is tested with a pure resistive load, consisting of oil filled radiators[11]. Four 2 kW radiators are parallel connected for each phase and the three phases are Y-connected. The loads can be adjusted so that the desired resistance is achieved. The experimental setup and the generator characteristics are thoroughly described in paper VI. For the second generator, a new measurement system is under development that will record longer time-series. Furthermore, it will be carefully calibrated to reduce the measurement error. The accuracy of the measurements on the first generator are discussed in paper VII.

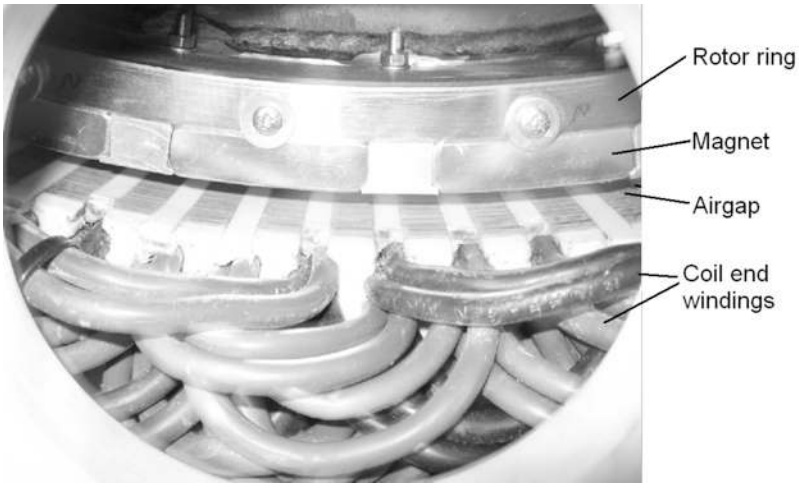

Figure 4.6: Close view of the generator taken on the first experimental generator.

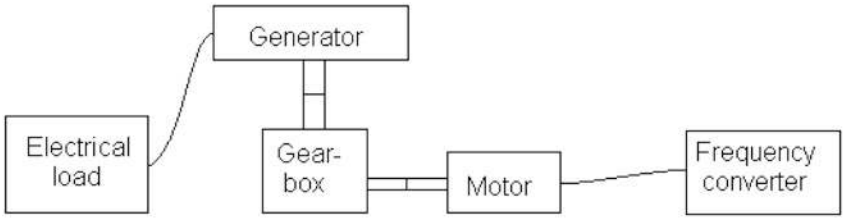

Figure 4.7: Sketch of the experimental setup.

[8] TDS 2024 and TPS 2014 from Tektronix with four channels each.
[9] Voltage probe Tektronix P2220.
[10] Measured as voltage over a current shunt of the type Cewe Instrument shunt 6112.
[11] Electric radiator heaters of type CZ-190820E from Duracraft.

4.2.2 VAWT setup and experiments

The construction of a VAWT was finalised in December 2006, see fig. 4.8. It is a 12 kW straight-bladed Darrieus turbine with a cross section area of 30 m^2 and a hub height of 6 m, see table 4.2 for further specifications. The generator is placed in the generator housing on ground level after being tested in the laboratory, see paper VI and VII. The drive shaft is enclosed by a tubular tower and directly connected to the generator rotor. Strain gauges[12] have been placed on the shaft to measure the torque. The VAWT design is further described in paper III and the construction and the first experimental results are presented in paper IV. It is situated at Marsta Meteorological Observatory outside of Uppsala, which is a well characterized wind site where wind measurements have been performed since 1994. A presentation of the mechanical design of the tower and foundation of the wind turbine can be found in [102].

Table 4.2: *Data for the VAWT.*

Rated rotational speed (rpm)	127
Rated blade tip speed (m/s)	40
Rated wind speed (m/s)	12
Number of blades	3
Cross section area (m^2)	30
Hub Height (m)	6
Turbine radius (m)	3
Blade Length (m)	5
Chord length (m)	0.25
Solidity	0.25
Aerodynamic control	Passive Stall
Blade Airfoil Section	NACA0021

The turbine is placed close to a building where all the electrical equipment is kept. The resistive electrical load consists of 12 electrical radiators, which previously were used for the first generator experimental setup, see section 4.2.1. The generator AC output was directly connected to the switchable loads to get the first experimental results presented in paper IV. Since then, a control system has been developed. The AC output is rectified and the electrical radiators are used as a DC load. The voltage level, and thereby also the rotational speed, can be controlled manually, see paper V. The next step under development is an automatic control system enabling the turbine to be run without supervision. Furthermore, a computer based measurement system using a DAQ card has recently been developed. For the first experimental data

[12] Two sets of strain gauges of the type QFCT-2-350-11-6F-1LT.

presented in paper IV, probes[13] were used to measure the currents[14] and voltages. The rotational speed was found from the electrical frequency. The probes were connected to two oscilloscopes[15]. The oscilloscopes could save a limited number of data points so only short time measurements could be performed. For the new measurement system the voltages and currents are measured with LEM transducers[16] in order to avoid electrical interference.

The VAWT is not self-starting and an auxiliary winding is included in the stator of the generator, which can be used as a start motor. The auxiliary winding has to be fed with an AC voltage adopted according to the poles of the generator in order to make it spin. Hall latches placed in the generator airgap gives feedback to the start circuit, see paper V.

A cup anemometer[17] mounted on a five meter pole is used to measure the wind. The anemometer is portable and is placed in front of the turbine depending on wind direction. However, the wind direction usually fluctuates and changes direction. The distance between the anemometer and the wind turbine is measured and the wind speed data is analysed with a time delay in order to compare it to the wind turbine output.

Figure 4.8: The VAWT.

[13] Voltage probe Tektronix P2220.

[14] Measured as voltage over a current shunt of the type Cewe Instrument shunt 6112.

[15] TDS 2024 and TPS 2014 from Tektronix with four channels each.

[16] LEM Current transducer HAL 50-S and LEM Voltage transducer LV25-P.

[17] Type VAISALA WMS302.

5. Summary of results and discussion

5.1 Generator design and simulations

Several generators have been designed using the simulation method described in section 4.1.1. The design of a 100 kW generator is presented in paper II. The design of a 12 kW generator is described in paper III and VI. The latter generator has been constructed according to the design. The magnetic flux density in the 12 kW generator from simulations can be seen in fig. 5.1. Furthermore, several 50 kW generators have been designed in paper VIII. The presented generator designs show direct driven PM synchronous generator designs for VAWTs, which all have a high efficiency and an acceptable size.

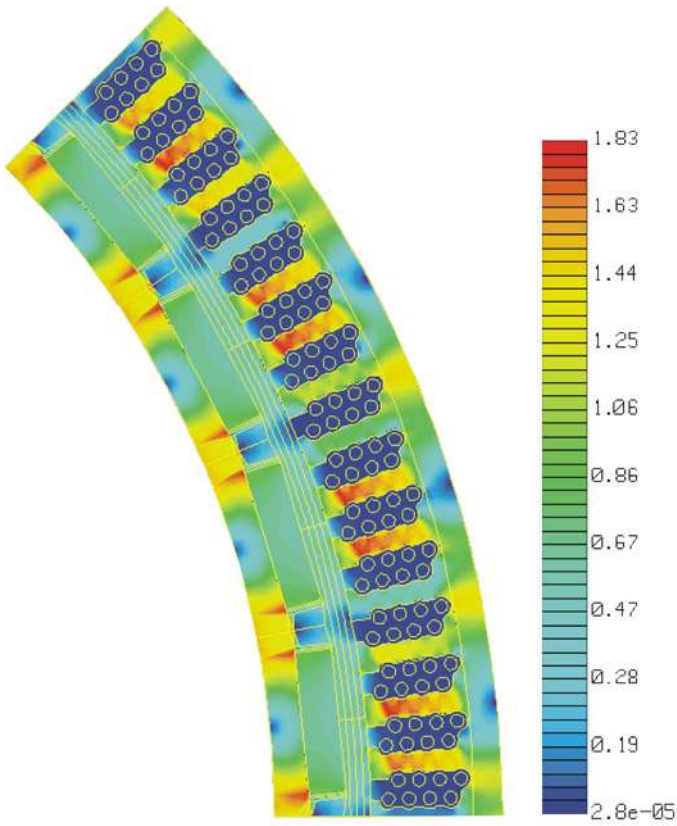

Figure 5.1: Magnetic flux density shown for one section of the 12 kW generator. The scale is in Tesla.

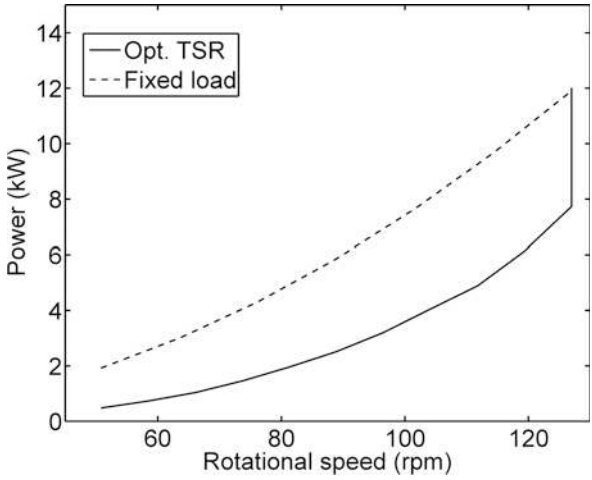

Figure 5.2: Simulated results of power as a function of rotational speed, for both operation at optimum TSR and operation with a constant resistive load.

In paper II, an analytical description of the 100 kW generator has been included, as described in section 3.3.2. The results show that the voltage requirement sets the dimensions of the machine, i.e. a more compact machine had been achieved if a lower voltage had been used. However, it is not desired to decrease the voltage level since this would venture overload capacity as well as increase the resistive losses.

It is important to test a designed generator as it will be used in a variable speed wind turbine and not only for a constant resistive load in order to study the behaviour of the generator. The 12 kW generator has been simulated for different loading conditions according to operation at optimum tip speed ratio, as the generator will be run when mounted in a wind turbine. For this design, the rotational speed will be held fixed at wind speeds above 10 m/s. The rated wind speed is 12 m/s. Results comparing power output at optimum TSR and at simulations for constant resistive load is shown in fig. 5.2. The figure indicates that the rotational speed will be different for a given power level depending on if the electrical load is controlled or constant.

In paper VIII, six generators are compared to each other. A number of characteristics are held constant in the six generators and the rated voltage is increased. The resulting trends in different characteristics can be seen in table 5.1. It can be seen that the PM weight is constant whereas the total generator weight is decreased. The load angle is decreased when the rated voltage is increased, indicating a better overload capability for higher rated voltage. The iron losses are increased with increasing rated voltage since the frequency is increased, whereas the copper losses are decreased due to the lower current.

Table 5.1: *Results from simulations of six generators for increasing rated voltage. The arrows indicate trends.*

Changed characteristic	**Trend**
Line voltage (V)	$\Uparrow$
Fixed characteristics	**Trend**
Power (kW)	$\rightarrow$
Rotational speed (rpm)	$\rightarrow$
Current density (A/mm^2)	$\rightarrow$
Slots per pole and phase	$\rightarrow$
Length to diameter ratio	$\rightarrow$
B airgap (T)	$\rightarrow$
B tooth (T)	$\rightarrow$
B yoke (T)	$\rightarrow$
Number of cables	$\rightarrow$
Resulting characteristics	**Trend**
Current (A)	$\downarrow$
Electrical frequency (Hz)	$\uparrow$
Number of poles	$\uparrow$
Magnet geometry (mm)	$\downarrow$
Stator inner diameter (mm)	$\uparrow$
Stator outer diameter (mm)	$\uparrow$
Airgap width (mm)	$\downarrow$
Generator length (mm)	$\uparrow$
Conductor area (mm^2)	$\downarrow$
Load angle ($^\circ$)	$\downarrow$
Steel weight (kg)	$\rightarrow$
Cable weight (kg)	$\downarrow$
PM weight (kg)	$\rightarrow$
Total weight (kg)	$\downarrow$
Iron losses (kW)	$\uparrow$
Copper losses (kW)	$\downarrow$

5.1.1 Electromagnetic losses

The six generators from paper VIII are compared considering efficiency and overload capability. A program was written that simulated a generator under variable speed operation using realistic control rules and stall regulation of the turbine to limit the power. A Rayleigh distributed wind speed was assumed. The results give the statistical distribution of the iron and copper losses in the generator which can be seen in fig. 5.3 together with the actual losses at different wind speeds for one of the simulated generators. The iron losses seem to have a small influence on the total losses when looking at the figure to the left. However, the right figure shows that the iron losses have a larger influence on the total losses than expected, due to the dominating low wind speeds.

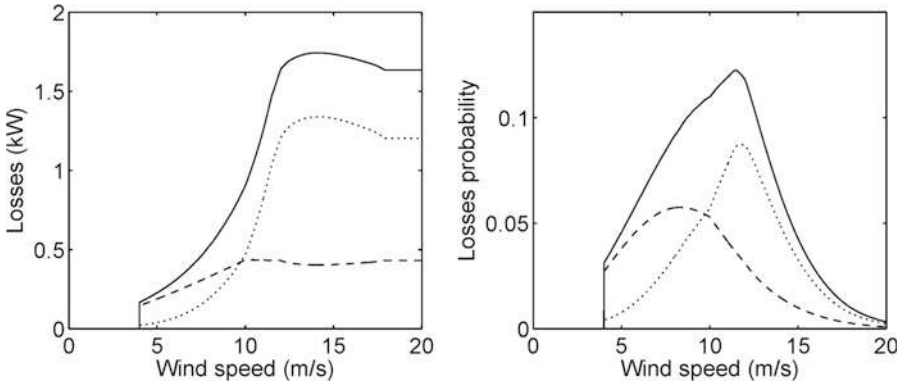

Figure 5.3: Results for a 50 kW generator rated at 334 V. To the left: The generator losses at different wind speeds. To the right: The probability of losses at different wind speeds at a mean wind speed of 7 m/s. The solid lines represent the total losses, the dashed lines represent the iron losses and the dotted lines represent the copper losses.

A comparison is performed between the six generators using the calculated average losses. The generators are defined by their different rated voltage level. Depending on the mean wind speed at the specific site, different results for the efficiencies are found, see fig. 5.4. The rated efficiencies differ from the results for the average efficiencies, especially at low average wind speeds. The overload capability is also compared by calculating the pull-out torque for the six generators, see fig. 5.5. It can be seen that the overload capability increases with higher rated voltage.

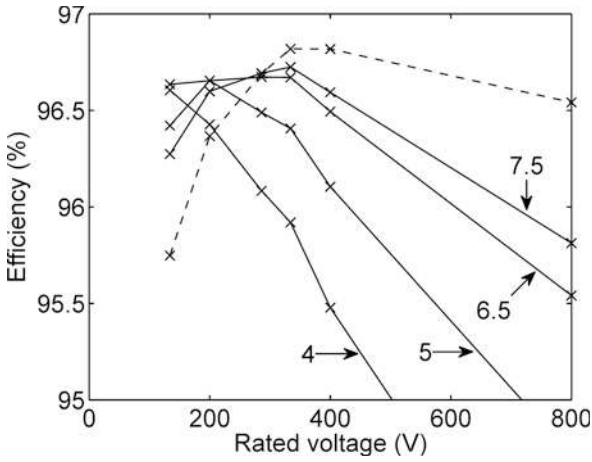

Figure 5.4: The rated efficiency (dashed) and the average efficiencies (solid) at different average wind speeds. The average wind speeds are shown in the figure (m/s).

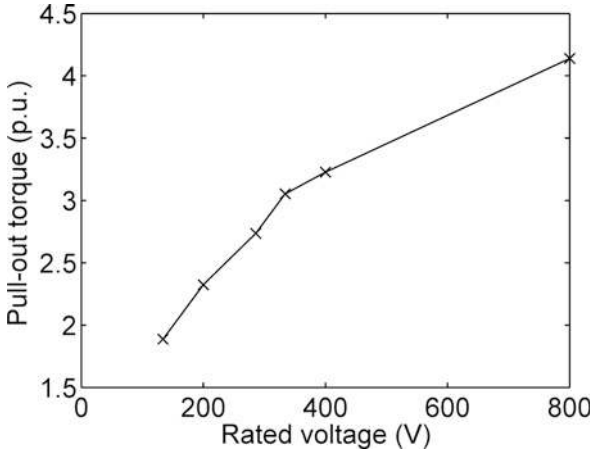

Figure 5.5: Pull-out torque in per unit of rated torque for the six generators.

5.2 Torsional vibrations

In paper II, the torsional vibrations of the drive shaft are studied for a vertical axis wind turbine. The use of a direct driven generator and a geared generator is compared in the aspect of torsional vibrations of the drive shaft. In fig. 5.6 the eigen frequency of vibrations for the two cases and the rotational frequency for the shaft is shown. The eigen frequency of the vibrations for the geared generator is dangerously close to the rotational speed, whereas the direct driven generator would ensure safe operation. In order to use the geared generator a thicker shaft must be used. It is concluded that the shaft mass in this case can be reduced by 42 per cent by using a direct driven generator. However, when studying torsional vibrations, a two-mass model would be more correct to use than the simplified one-mass model used here.

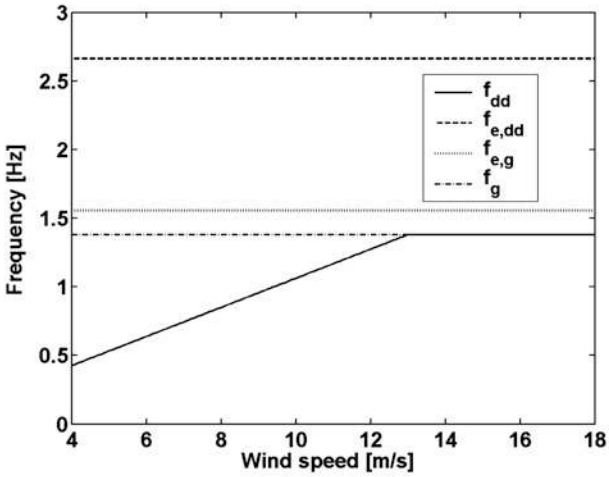

Figure 5.6: Frequency diagram for two different generators, which shows the eigen frequencies (direct-drive, $f_{e,dd}$, geared, $f_{e,g}$) and the shaft rotational frequencies (direct-drive, f_{dd} and geared, f_g).

5.3 Experimental results for the generator

The 12 kW generator which has been designed and constructed works satisfactory, see paper V, VI and VII. Experimental results for the generator have been compared with dynamic simulations, see table 5.2. Results from experiments correspond closely to simulations. However, the experimental voltage and current are slightly lower than expected from simulations.

The simulated and the experimentally obtained phase voltages show good correspondence, see fig. 5.7. Both curves have a shape that is similar to a sine wave. However, the curves are slightly flatter, due to the third harmonic. The harmonics present in the voltages can be seen in fig. 5.8. Most harmonics have

Table 5.2: *Results from dynamic simulations and experiments at rated conditions.*

	Dynamic simulation	**Experiment**
Power (kW)	12.2	11.4
Phase voltage (V) rms	162.6	157.1
No load phase voltage (V) rms	-	161.3
Current (A) rms	25.0	24.2
Electrical frequency (Hz)	33.9	33.9
Rotational speed (rpm)	127	127
Electrical load (Ω)	6.5	6.5
Phase angle (°)	0	0
Inner resistance (Ω)	0.155	0.151

a very low occurrence in the phase voltage apart from the third harmonic. The 7th harmonic is present but fairly low. The results correspond to what was expected from simulations, see paper VI. The third harmonic is present in the phase voltage but will be suppressed in the line voltage. In the phase voltage, the third harmonic is from experiments 5.75 % and from simulations 5.6 %, given in percentage of the fundamental tone, which is 100 % by default. Furthermore, the experimental 7th tone is 0.21 % and from simulations 0.3 %.

The power obtained from experiments and the simulated power is compared in fig. 5.9. The experimental power is lower than the simulated power, as was expected since both voltage and current were lower in the experiments.

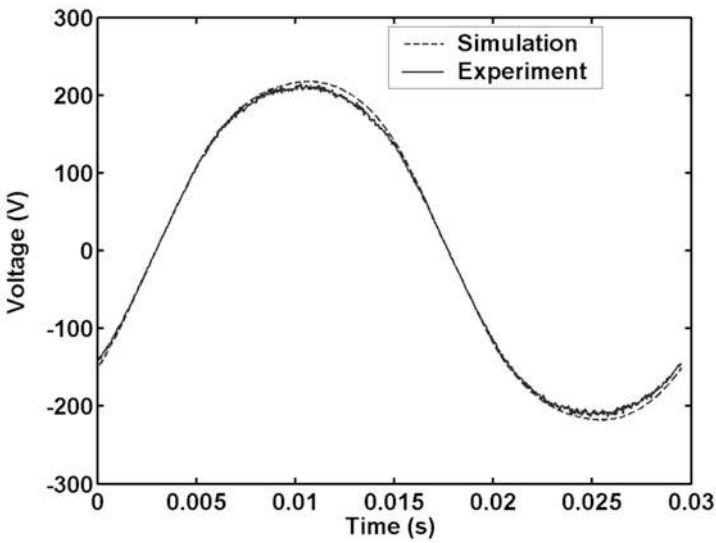

Figure 5.7: The phase voltage as a function of time from experiments and simulations.

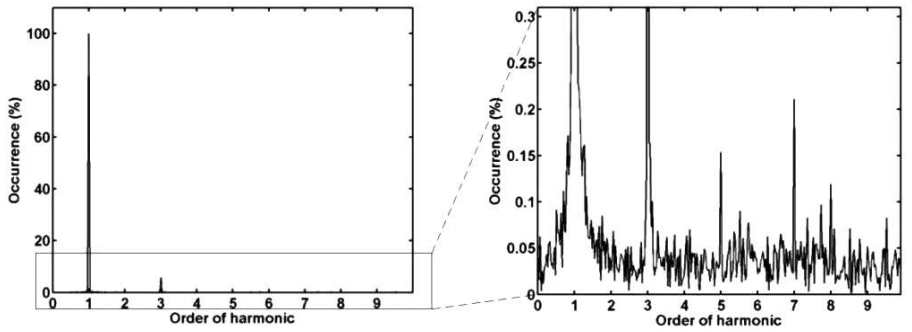

Figure 5.8: Harmonics for the experimental load phase voltage displayed as a function of the order of harmonic. The occurrence is presented as per cent of the first harmonic. The two figures show the same results with different scales.

These deviations probably have to do with differences between the experimental setup and the simulated generator as discussed in paper VI. One phase of the generator is delivering slightly less power than the others, which might explain why the experimentally obtained power curve has an uneven shape. The fluctuations in the power outputs are due to the harmonics.

The generator has also been tested for different loads and different rotational speeds. The results have been compared to simulations and the measurement errors on the experimental results have been calculated and displayed as error bars, see fig. 5.10. The measurements correspond well with simulations. The armature reaction can be seen in fig. 5.10b). It is shown that the voltage drop is rather small, showing that the machine reactance in the generator is low, which is a good characteristic.

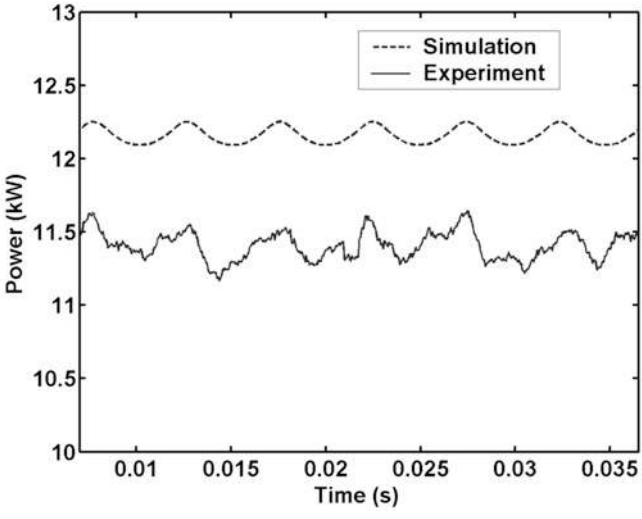

Figure 5.9: The total power from experiments and from simulations.

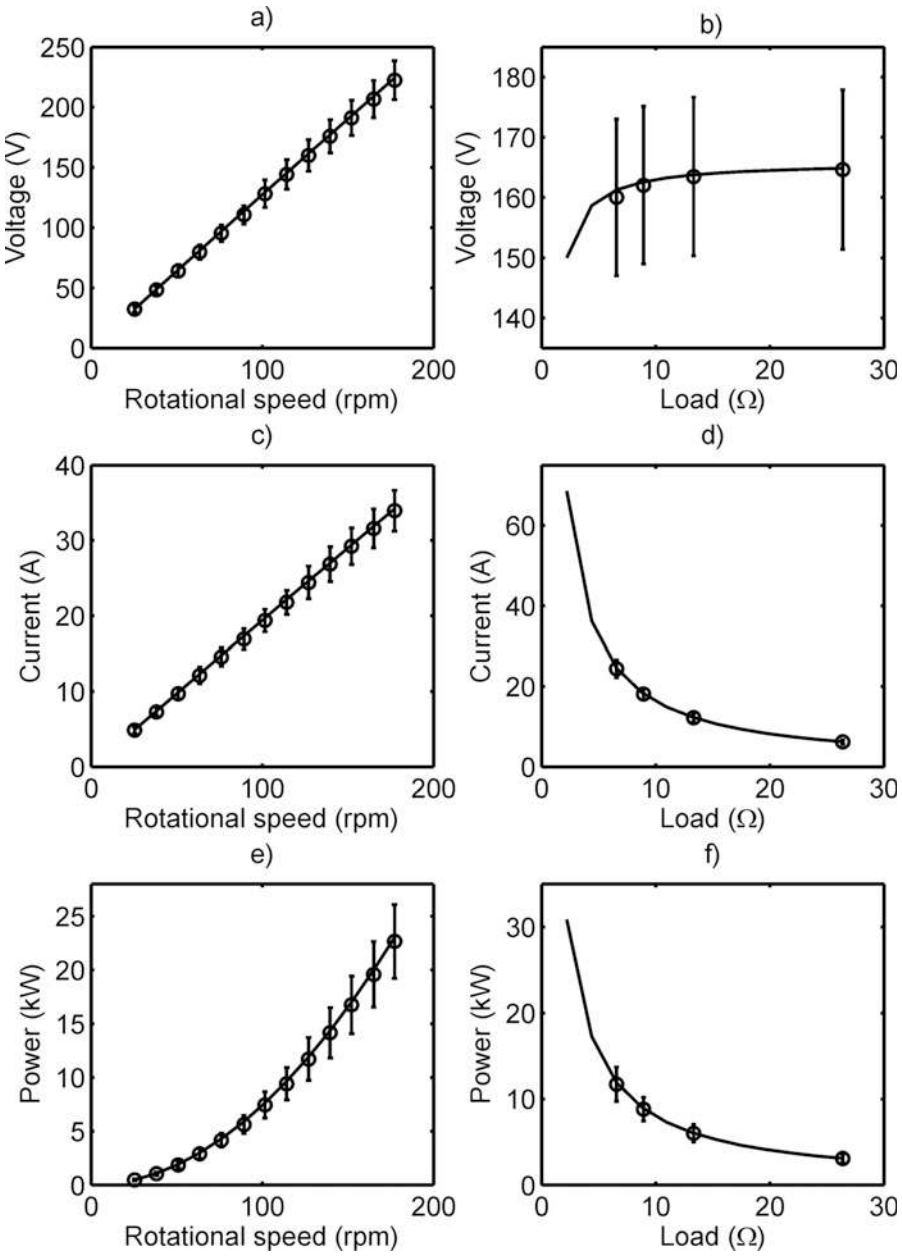

Figure 5.10: The left-hand figures show voltage, current and power as a function of rotational speed for constant resistive load of 6.5 Ω. The right-hand figures show voltage, current and power for changing load at constant rotational speed of 127 rpm. The solid lines are results from simulations and the dots represent experimental results. The error bars represent the accuracy of the measurement and indicate possible maximum and minimum values of the measured variable.

5.4 Experimental results for the VAWT

The constructed VAWT has been tested experimentally. The first tests were performed during a highly turbulent day and the results are presented in paper IV. An example of the power absorption can be seen in fig. 5.11, where a power of 4 kW is reached momentarily. The C_P, calculated for a large number of measurements, is presented in fig. 5.12. However, these data are taken for short time intervals, which might deteriorate the results. The results between a TSR of 3 and 4 are considered most reliable. A couple of curve fittings have been included in the figure for comparison. The curve fittings indicate a higher optimum TSR than 4, as was expected from simulations, see paper III.

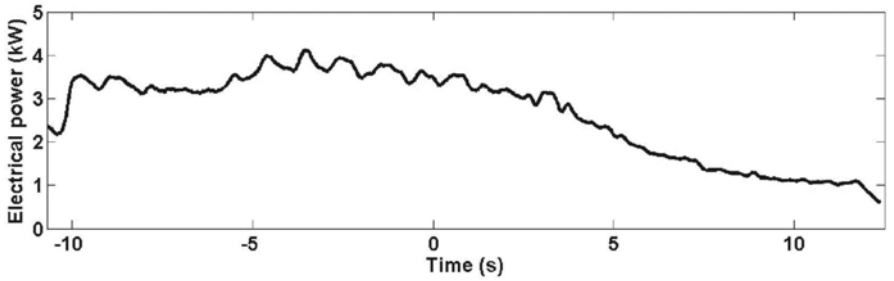

Figure 5.11: The power from the VAWT.

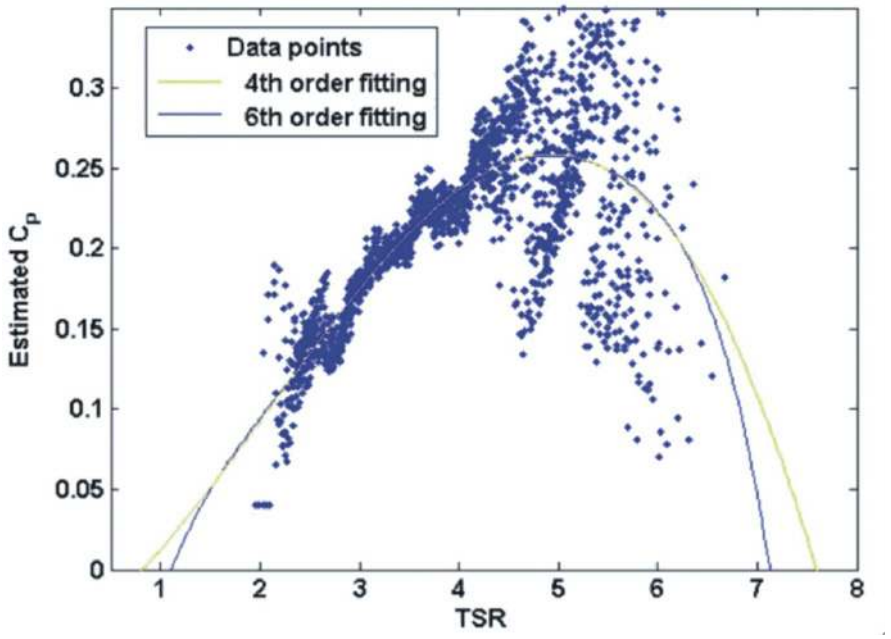

Figure 5.12: The power coefficient as a function of the tip speed ratio.

A control system and a start up system was developed, see paper V. The control system will electrically control the rotational speed of the wind turbine so it can be run at a variable speed adjusted to the varying wind speed, see section 3.2.2. The control system manages to keep the rotational speed constant when the wind speed changes, see fig. 5.13. The rotational speed was adjusted manually but an automatic control system is under development.

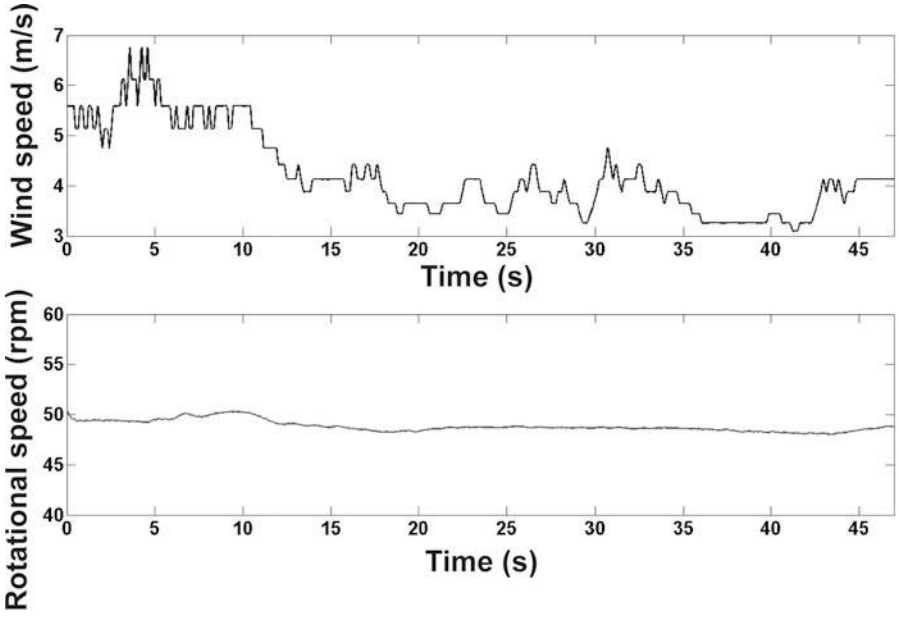

Figure 5.13: The rotational speed held constant by the control system.

6. Conclusions

The demand for a reliable wind power technique with a minimized need for maintenance, yields an interest in investigating different options for wind power. The wind turbine business in the world today mostly revolves around horizontal axis wind turbines with pitch control and a geared generator. Here, the option to use a vertical axis wind turbine with a direct driven generator has been explored. This thesis is focused on PMSGs for VAWTs. A cable wound PMSG used together with a straight-bladed VAWT represents a novel concept. The concept has been investigated both with simulations and through experiments. The strength of the H-rotor concept is the possibility to keep the structure simple. The H-rotor does not require any yaw mechanism, pitch regulation or gearbox and therefore has few movable parts, which is expected to demand less maintenance.

Several generators have been designed using the same FEM based simulation method. In particular, the design concerning a 12 kW generator has been in focus as a case study allowing general conclusions for PMSGs for VAWTs. The 12 kW generator has been designed to rotate with 127 rpm at rated power and to have a rated phase voltage of 156 V. It has been designed with 16 pole pairs and a height to diameter ratio in the airgap of 0.30. A theoretical electrical efficiency at rated power of 94.8 per cent has been achieved. All constructional challenges have been solved and an experimental setup have been finalised. The generator has been adapted to the vertical axis wind turbine and dimensioned to handle both mechanical and thermal overload, which has been possible thanks to elaborate FEM simulations of the generator electromagnetic design. The simulations indicate possibility of implementing a generator controlled stall regulation to limit power absorption for high wind speeds.

The generator has first been tested at rated power. Special attention has been paid to the waveform of the voltage, i.e. the harmonic content of the output. Furthermore, the generator has been tested for different rotational speeds (0.2 to 1.4 p.u.) and different resistive loads (1.08 to 4.34 p.u.). The results from the experiments on the prototype have been compared with FEM simulations. The high agreement between experimental results and FEM based simulations confirm the accuracy of the simulations. The generator will be run at optimum TSR in the wind turbine for the turbine to absorb the most power. The high agreement between simulations and experiments during experiments at varied speed and load, leads to the conclusion that the simulated results for opti-

mum TSR should be applicable also to the experimental generator. According to simulations, the 12 kW generator has a high overload capability and high electromagnetic efficiency. Together with values from simulations for optimum TSR, the generator can be said to be well characterised. The tested generator is currently used in a wind turbine. To correctly analyze results from the operating wind turbine it was important to test the generator extensively before mounting it in the wind turbine. In addition, the experimental setup for the new, identical generator can be used for more extreme generator tests such as long-term overload tests as well as short-circuit tests.

The design of a 12 kW VAWT has been completed and the VAWT has been constructed accordingly. The first experimental data in terms of generated electrical power and aerodynamic efficiency show promising results. A C_P of 0.23 has been found at a TSR of 4 for highly turbulent wind conditions. It has been shown that a vertical axis wind turbine can be controlled electrically through the generator. Furthermore, with an electric drive circuit and an auxiliary winding the wind turbine does not need to be self starting.

A method to calculate the yearly average of electromagnetic losses in a generator has been presented. The method takes the statistical wind distribution, control scheme and aerodynamic efficiency (C_P-TSR dependency) into consideration in order to evaluate the losses properly. It has been shown that the iron losses usually are larger when looking at the average losses as compared with the losses at rated speed. This can be explained by common part load operation of the generator. However, optimizing a generator for high average efficiency might lower the overload capability. The design optimization process results in a compromise between maximizing the efficiency and having a high overload capability. The relation between iron losses and copper losses are roughly dependent on the relation between rated voltage and current. For a fixed output power the increase in rated voltage will give a larger machine volume, a higher frequency and thereby increased iron losses, whilst the current will decrease and thereby reduce the copper losses.

Torsional vibrations in the drive shaft of a VAWT have been studied. It has been shown that a direct driven synchronous generator is preferable to an induction generator connected through a gearbox. In the performed case study, the use of a direct driven generator would reduce the required shaft mass by 42 per cent.

7. Suggestions for future work

This project has recently started and there are a large number of interesting things to study. A few of those are suggested below and some are already in the planning stage. This section covers suggestions for future work for the wind power project in general and not only direct continuation on the work presented here.

Further tests will be conducted on the generator experimental setup regarding the behaviour of the generator. Several specific experiments will be conducted such as torque measurement, short circuit tests, determining the pull-out torque and thermal overload investigation. The generator experimental setup will also be used for further calibration of the simulation method. Furthermore, a rectifier will be built for experiments.

When the long-time control and measurement systems for the VAWT are completed, the turbine will be running automatically and long-time tests will be performed on the wind turbine. These tests will give a more correct result on the C_P according to standards. Results from analyzing the generator in the laboratory will be useful at this stage. Several strain gauges have been mounted on the shaft of the wind turbine to measure the torque and detect vibrations. The torque will be measured and the torque harmonic content will be decomposed and analysed in terms of eigen frequencies. When the torque measurement system is completed the wind turbine can be used to calibrate the aerodynamic model. The wind turbine experimental setup will also be improved by the development of a more complex wind speed measurement system to give better measurements of turbulence. The system will give better data on how the turbine responds to turbulent winds, changes in wind direction and gusts.

Several studies based on simulations can be performed with the powerful FEM simulation method, for instance a deeper study on different generator losses and on design optimization. Furthermore, rectification could be included in the simulations to develop a model for the electrical system.

A two-mass model to study torsional vibrations could be developed. Vibrations should be studied for all different triggering frequencies, transients etc. Furthermore, a "wind to grid" model should be developed in order to study dynamical interaction with the electrical system and the grid.

8. Summary of papers

All the work presented here is based on the same concept, an H-rotor with a direct driven PM synchronous generator. The papers can be divided into two parts, where the first part deals with the whole wind turbine and the second part is more focused on the generator. Paper I motivates the choice of the H-rotor concept by comparing different types of turbines from many different points of view. This paper also includes a review of previous VAWT projects. Paper II deals with the drive train of a VAWT and motivates the use of a direct driven generator instead of a geared generator. This theoretical paper studies vibrations in the drive shaft connecting the turbine to the generator. Paper III, IV and V are conference papers describing the development of the vertical axis wind turbine prototype: from design to experimental results and development of a control system.

Paper VI presents the generator design and the experimental setup as well as the first experiments. Paper VII presents results on further experiments on the generator that were performed in the laboratory before the generator was mounted in the VAWT. In both these experimental papers the results from experiments have been compared to simulations. Paper VIII is a theoretical study of electromagnetic losses in generators and discusses how to optimize the generator efficiency.

The author's contribution to each paper is given below. For all papers, the planning and interpretation have been done together with the co-authors.

Paper I

Evaluation of different turbine concepts for wind power.

This is a review paper focusing on the differences between vertical axis wind turbines and horizontal axis wind turbines. A historical background and a short review of active VAWT projects are presented. Two different types of VAWTs are compared to HAWTs. The paper aims at making a comparative study of these three different wind turbines from different aspects including structural dynamics, control systems, maintenance, manufacturing, electrical equipment, environmental impact and cost. A case study is presented where three different turbines are compared to each other. Furthermore, a study of the size of blade areas for different turbines is presented. The vertical axis wind turbine appears to be advantageous to the horizontal axis wind turbine in several aspects.

The author has done the review and the case studies. The comparative study was performed together with the co-authors. The author has written the whole paper.

Published in *Renewable and Sustainable Energy Reviews*.

Paper II

Generator-damped torsional vibrations of a vertical axis wind turbine.

In this paper, torsional vibrations of the drive shaft of a VAWT are studied. First, the design of a 100 kW generator is presented, which is suggested to be used together with a specified VAWT. The simulation method described in section 4.1.1 has been used. Second, another option of a generator is presented, which is an induction generator with a gearbox. Finally, the two generators are compared concerning the risks for harmful torsional vibrations. Direct driven generators are shown to be preferred when torsional vibrations are considered, since the eigen frequency of the fundamental vibration is greater for a direct driven generator than for a geared generator. The generator damping of vibrations for the simulated, direct driven synchronous generator is also studied.

The intention with this paper is to show the difference between a direct driven generator and an induction generator with a gearbox, not to give a full description of shaft vibrations. The dynamic model used in this paper could be improved as was discussed in section 3.5.1.

The author has done the generator simulations. The dynamic calculations were done together with the co-author. The author has written the whole paper.

Published in *Wind Engineering*.

Paper III

Design of a 12kW vertical axis wind turbine equipped with a direct driven PM synchronous generator.

This paper describes the design of a complete 12 kW VAWT, from generator to blades. The electric design as well as aerodynamic and structural design has been performed using different simulation methods. For the generator design, the simulation method described in section 4.1.1 has been used.

The author has taken a major part in designing the generator and to some extent taken part in designing other parts of the turbine. The author has written part of the paper.

Presented with a poster at the *European Wind energy Conference & Exhibition 2006*.

Paper IV

Experimental results from a 12 kW vertical axis wind turbine with a direct driven PM synchronous generator.

This paper presents the construction of the generator and the complete 12 kW VAWT. It also presents the site where the turbine is situated, which has a well characterized wind climate. The data treatment method is explained. Experimental data on rotational speed and electrical power is presented. Furthermore, a preliminary C_P-TSR curve is presented with data from measurements on a day with high turbulence. These first experimental data is as expected considering the highly turbulent wind conditions.

The author has taken part in design and construction of the wind turbine. The author has taken part in experiments and data treatment. The author has written part of the paper.

Presented with a poster at the *European Wind energy Conference & Exhibition 2007*.

Paper V

Progress of control system and measurement techniques for a 12 kW vertical axis wind turbine.

This paper presents parts of the electrical system of the 12 kW VAWT. The first part is the voltage control load that keeps the rotational speed constant. The rotational speed is adjusted manually and can be adapted to the prevailing wind conditions. The second part of the electrical system is the electrical starter, which accelerates the turbine until it is rotated by the wind. The paper includes experimental results showing control of the rotational speed, both during operation and during start-up. Furthermore, the paper presents the measurement system that is under development.

The author has taken part in design and construction of the wind turbine. The author has taken a small part in developing the load control system and taken part in experiments and data treatment. The author has written part of the paper.

Presented orally by J. Kjellin at the *European Wind energy Conference & Exhibition 2008*. Published in proceedings. Reviewed conference paper.

Paper VI

Simulations and experiments on a 12 kW direct driven PM synchronous generator for wind power.

This paper presents measurements on the constructed generator, with the design presented in paper III. The generator design and characteristics are presented as well as the experimental setup. The first experimental results for

rated speed are presented. The voltage is analysed considering harmonics and the results are compared to simulations. The simulation method described in section 4.1.1 is used. The generator works as expected and the experimental results are in good agreement with simulations.

The author has taken a major part in designing the generator. The author has taken part in constructing the generator and in preparing the experimental setup. The author has performed all the experiments and simulations and written the whole paper.

Published in *Renewable Energy*.

Paper VII

FEM simulations and experiments of different loading conditions for a 12 kW direct driven PM synchronous generator for wind power

The generator that has been presented in paper VI is here studied further. The generator has been tested with different loads and at different speeds. The results from experiments correspond well with simulations. The measurement errors in the experimental results are evaluated and the results are presented with error bars. Furthermore, the generator behaviour at operation at optimum tip speed ratio is investigated through simulations. The simulation method described in section 4.1.1 is used.

The author has taken a major part in designing the generator. The author has taken part in constructing the generator and in preparing the experimental setup. The author has performed all the simulations and written most of the paper.

Conditionally accepted for publication in *International Journal of Emerging Electric Power Systems*.

Paper VIII

Loss evaluation and design optimization for direct driven permanent magnet synchronous generators for wind power

This paper investigates electromagnetic losses in a permanent magnet synchronous generator. The iron losses and copper losses are compared. The average losses are calculated using the statistical wind distribution, the aerodynamic efficiency curve and a realistic operational scheme. A comparison is made with conditions at rated power. Furthermore, six 50 kW generators are designed with different rated voltage levels, which are compared considering losses. The simulation method described in section 4.1.1 is used for the electromagnetic simulations of the generators. The pull-out torque for all six generators is also calculated. The results show that it is important to consider the average losses and not only consider rated losses. It is concluded that the

design optimization process becomes a compromise between reducing the average losses and having a high overload capability.

The author has done all the simulations and written the whole paper.

Submitted in July 2008 to *IEEE Transactions on Energy Conversion*.

8.1 Errata to papers

1. In paper II, eqn (7) should be

$$M(t) = M_0 \sin(\omega t)$$

2. In paper II, p.452. The sentence before eqn (14): "The frequency of the tower movement is" should be replaced by "The rotational frequency of the shaft is".
3. In paper II, reference [22], the authors order should be: Roynarin,W., Leung, P.S. and Datta, P.K.
4. In paper III, p.6, eqn (1) should be

$$\sigma \frac{\partial A_z}{\partial t} - \nabla \cdot \left(\frac{1}{\mu_0 \mu_r} \nabla A_z \right) = -\sigma \frac{\partial V}{\partial z}$$

5a) In paper III, p.7, eqn (2), R_s^{end} should be replaced by R_s at all occasions. In the sentence below "R_s^{end} is the coil end resistance" should be replaced by "R_s is the cable resistance".
b) In paper VI, p.675, column 2, row 3-4, "R_s^{end} is the coil end resistance" should be replaced by "R_s is the cable resistance".
c) In paper VII, p.2, last row "R_s^{end} is the coil end resistance" should be replaced by "R_s is the cable resistance".
6. In paper III, p.7, table 2, row 2: "Phase voltage" should be replaced by "Line voltage".
7. In paper IV, p.10, reference [17] has not been published.
8. In paper VII, the acknowledgements[1] were not inserted in the submitted version of the paper. It will be included in the paper when it is published.

[1] Acknowledgements: Funding agencies Stiftelsen Olle Engkvist Byggmästare, Civilingenjörsförbundets Miljöfond, Swedish Energy Agency and VINNOVA are acknowledged for contributing funds making this work possible. Furthermore, Draka Kabel AB and SKF are acknowledged for contributions. Dr. A. Wolfbrandt and Dr. K.E. Karlsson are acknowledged for assistance with electromagnetic FEM modelling of generator. Erik Brolin and Paul Deglaire are acknowledged for their work with the experimental setup. Andreas Solum is acknowledged for good collaboration with setting up the experiment and obtaining experimental data.

9. Acknowledgements

Ett stort tack till...

... min handledare Hans Bernhoff för bra handledning, stöd och uppmuntran samt för din stora entusiasm för vindprojektet.

... min biträdande handledare Mats Leijon för att jag har fått möjligheten att doktorera i detta intressanta projekt, för intressanta diskussioner samt för att du skapat en bra atmosfär på denna arbetsplats.

... Energimyndigheten och VINNOVA för finansieringen av mitt arbete inom Centrum för Förnybar Elenergiomvandling (CFE).

... Arne Wolfbrandt, Karl-Erik Karlsson och Urban Lundin för utveckling, programmering och stöd med simuleringarna. Tack även till Urban för att du svarat på alla generatorfrågor.

... Gunnel, Christina, Ingrid Ringård, Ulf och Thomas för allt det praktiska som ni sköter så bra.

... vindgruppen för gott samarbete: Jon, Fredrik, Anders, Magnus, Micke och Marcus, tidigare kollegorna Paul och Andreas samt alla exjobbare och sommarjobbare som slitit med experimentuppställningarna under åren.

... Hans, Mats, Micke, Arne, Karin, Jon och Fredrik för att ha läst delar eller hela min avhandling. Tack även till fotograferna Jon och Hans för fina omslagsbilder.

... alla på avdelningen för elektricitetslära för gott samarbete genom åren och framförallt för att ni är de bästa arbetskamrater jag kan tänka mig. Speciellt tack till Mårten för initiativet till fredagsöl!

... Karin för att du ledde in mig på den här vägen till att börja med (jag hade nog inte doktorerat om det inte vore för du), för att du har varit ett stöd som jobbarkompis under denna tidsperiod och framförallt för att du är en bra vän.

Avslutningsvis, tack till...

... familj och vänner för att ni är så bra och för att ni alltid finns där för mig.

... Yvonne och Lucia. Utan er hade det inte blivit någon avhandling (i alla fall ingen som handlar om er!). Och tack till Lucia för att du gick med på att vara cover girl.

10. Summary in Swedish

Direktdrivna generatorer för vertikalaxlade vindkraftverk

Vinden är en förnybar energikälla som har använts av människor under lång tid, exempelvis i segelbåtar. Man började omvandla vindenergi till elektricitet i slutet av 1800-talet men det är inte förrän på 70-talet som den stora utbyggnaden av vindkraftverk påbörjades. Idag bygger de flesta länderna i EU ut vindkraften. Den traditionella vindkraften består av en teknik som utvecklades i Danmark på 80-talet och består av en trebladig horisontalaxlad turbin, en växellåda och en snabbroterande generator.

Tekniken som utvecklats vid avdelningen för elektricitetslära består av en vertikalaxlad turbin med en direktdriven generator som är placerad på marknivå. På så sätt behöver man inte ha en växellåda som kan ge förluster och kräva underhåll eller i värsta fall gå sönder. En vertikalaxlad turbin har fördelen att den inte är beroende av vindriktning för att kunna rotera. Den behöver alltså inte giras in mot vinden såsom ett traditionellt horisontalaxlat vindkraftverk behöver göras.

Fokus i denna doktorsavhandling ligger på generatorn. Denna generator är en direktdriven, och därmed långsamtgående synkron elektrisk maskin. Den har en kabellindad stator och rotorn är permanentmagnetiserad. Generatorn har designats och studerats med hjälp av en simuleringsmetod som innebär att fältekvationer kopplas med kretsekvationer. Det komplexa problemet löses med hjälp av finita elementmetoden. Med den utvecklade simuleringsmetoden kan man både optimera en design samt göra simuleringar på en fix design och exempelvis studera olika lastfall.

En 12 kW generator har designats och konstruerats. En komplett experimentuppställning har färdigställts och experiment har verifierat simuleringarna. Tester har gjorts vid olika laster och rotationshastigheter. Dessutom har förekomsten av övertoner analyserats. Generatorn fungerar som förväntat och de experimentella resultaten stämmer väl överens med simuleringarna.

Förluster och verkningsgrad på denna typ av generator har studerats med hjälp av simuleringar. Förlusterna i olika delar av generatorn undersöktes, det vill säga järnförluster i statorstålet och kopparförluster i kablarna. Det visar sig att järnförlusterna vanligen blir dominerande vid låga vindhastigheter medan kopparförlusterna växer snabbt vid höga vindhastigheter.

Inom projektet har även en 12 kW prototyp av ett vindkraftverk konstruerats och testats. De första experimentresultaten visar att det fungerar som förvän-

tat. Ett kontrollsystem har utvecklats till vindkraftverket för att det ska kunna användas optimalt, det vill säga att rotationshastigheten ska vara optimalt anpassad efter rådande vindhastighet vid normaldrift.

De två experimentuppställningarna ger goda möjligheter att fortsätta undersökningen av konceptet med ett vertikalaxlat vindkraftverk med en direktdriven generator i framtiden.

References

[1] F. Robelius. Giant oil fields - the highway to oil. ISBN 978-91-554-6823-1, Uppsala, Sweden, 2007. Ph.D. dissertation, Digital comprehensive summaries of Uppsala dissertations from the faculty of science and technology.

[2] L. Bernstein *et al. IPCC, 2007: Climate Change 2007: Synthesis Report. Contribution of Working Groups I, II and III to the Fourth Assessment Report of the Intergovernmental Panel on Climate Change*. Core Writing Team, R.K. Pachauri and A. Reisinger (eds.), IPCC, Geneva, Switzerland, 2007.

[3] BTM Consult ApS. *International wind energy development - World market update 2007*. BTM Consult Aps., I. C. Christensens Allé 1, DK-6950 Ringkobing, Denmark, 2008.

[4] Anon. Wind force 10. A blueprint to achieve 10% of the world's electricity from wind power by 2020. EWEA, Rue d'Arlon 63-65, B-1040 Brussels, Belgium, 1999. EWEA report.

[5] O. Ågren, M. Berg, and M. Leijon. A time-dependent potential flow theory for the aerodynamics of vertical axis wind turbines. *J. Appl. Phys.*, 97:104913, 2005.

[6] P. Deglaire, O. Ågren, H. Bernhoff, and M. Leijon. Conformal mapping and efficient boundary element method without boundary elements for fast vortex particle simulations. *European Journal of Mechanics B/Fluids*, 27:150 – 176, 2008.

[7] A. Solum and M. Leijon. Investigating the overload capacity of a direct-driven synchronous permanent magnet wind turbine generator designed using high-voltage cable technology. *International Journal of Energy Research*, 31(11):1076 – 1086, 2007.

[8] A. Solum. Permanent magnet generator for direct drive wind turbines. UURIE 303-06L, ISSN 0349-8352, Division for Electricity, Box 534, 75121 Uppsala, Sweden, 2006. Licentiate Thesis.

[9] A. IIda, A. Mizuno, and K. Fukudome. Numerical simulation of aerodynamic noise radiated form vertical axis wind turbines. Kyoto, Japan, 2004. Proc. of ICA 2004, The 18th International Congress on Acoustics.

[10] J. Ribrant and L.M. Bertling. Survey of failures in wind power systems with focus on Swedish wind power plants during 1997-2005. *IEEE Transactions on Energy Conversion*, 22(1):167 – 173, 2007.

[11] C. Brothers. Vertical axis wind turbines for cold climate applications. Montreal, Canada. Renewable Energy Technologies in Cold Climates '98 International Conference.

[12] W. Roynarin, P.S. Leung, and P.K. Datta. The performances of a vertical darrieus machine with modern high lift airfoils. Newcastle, UK, 2002. Proceedings from IMAREST conference MAREC.

[13] S. Angelin *et al. Hydropower in Sweden*. The Swedish Power Associaton and The Swedish State Power Board, The Swedish Power Association, Box 1704, 111 87 Stockholm, Sweden, 1981.

[14] S. Jöckel. Gearless wind energy converters with permanent magnet generators - an option for the future? Göteborg, Sweden, 1996. Proc. European Union Wind Energy Conference, EWEA.

[15] M. Dahlgren, H. Frank, M. Leijon, F. Owman, and L. Walfridsson. Windformer - wind power goes large scale. *ABB Review*, 3:31 – 37, 2000.

[16] D. Jiles. *Introduction to magnetism and magnetic materials*. CRC Press, Boca Raton, Florida, USA, 2^{nd} edition, 1998.

[17] M. Leijon, M. Dahlgren, L. Walfridsson, L. Ming, and A. Jaksts. A recent development in the electrical insulation systems of generators and transformers. *IEEE Electrical Insulation Magazine*, 17(3):10 – 15, 2001.

[18] T. Ackermann and L. Söder. An overview of wind energy-status 2002. *Renewable and Sustainable Energy Reviews*, 6(1 – 2):67 – 127, 2002.

[19] G.M. Joselin Herbert, S. Iniyan, E. Sreevalsan, and S. Rajapandian. A review of wind energy technologies. *Renewable and Sustainable Energy Reviews*, 11(6):1117 – 1145, 2007.

[20] Shikha, T.S. Bhatti, and D.P. Kothari. Early development of modern vertical and horizontal axis wind turbines: A review. *Wind Engineering*, 29(3):287 – 299, 2005.

[21] Anon. Turning wind power on its side. *Economist*, 378(8468):3 – 4, 2006.

[22] S. Peace. Another approach to wind (cover story). *Mechanical Engineering*, 126(6):28 – 31, 2004.

[23] H. Riegler. HAWT versus VAWT: Small VAWTs find a clear niche. *Refocus*, 4(4):44 – 46, 2003.

[24] J. Knight. Urban wind power: Breezing into town. *Nature*, 430(6995):12 – 13, 2004.

[25] Anon. Vertical axis wind turbines: The history of the DOE program. Wind Energy Technology Department, Sandia National Laboratories, PO Box 5800, Albuquerque, NM 87185, USA, 1987, http://www.sandia.gov/wind/images/VAWThist.html, retrieved 2008-07-18.

[26] J.F. Manwell, J.G. McGowan, and A.L. Rogers. *Wind energy explained*. John Wiley and Sons Ltd., Amherst, USA, 1st edition, 2002.

[27] S.J. Savonius. Rotor adapted to be driven by wind or flowing water. US Patent No. 1.697.574, 1929.

[28] G.J.M. Darrieus. Turbine having its rotating shaft transverse to the flow of the current. US Patent No. 1.835.018, 1931.

[29] J. German. The end of an era: Sandia's 17-meter vertical axis wind turbine comes down after two decades. Sandia National Laboratories, PO Box 5800, Albuquerque, NM 87185, USA, 1997. Sandia Lab News; LN11-21-97.

[30] D.R. Smith. The wind farms at Altamont Pass area. *Ann. Rev. Energy*, 12:145 – 183, 1987.

[31] S. Peace. Why not vertical axis? refocus 2003. *Refocus*, 4(3):30 – 33, 2003.

[32] P.W. Carlin, A.S. Laxson, and E.B. Muljadi. The history and state of the art of variable-speed wind turbine technology. National Renewable Energy Laboratory, Technical Report: NREL/TP-28607, 2001.

[33] P.J. Musgrove. Wind energy conversion: recent progress and future prospects. *Solar and Wind Technology*, 4(1):37 – 49, 1987.

[34] C.A. Morgan, P. Gardner, I.D. Mays, and M.B. Anderson. The demonstration of a stall regulated 100 kW vertical axis wind turbine. pages 645 – 649, Glasgow, Scotland, 1989. Proc. 1989 European Wind Energy Conference.

[35] I.D. Mays and C.A. Morgan. The 500 kW VAWT 850 demonstration project. pages 1049 – 1053, Glasgow, Scotland, 1989. Proc. 1989 European Wind Energy Conference.

[36] J. van Beek. Keeping antarctica pollution free. *Windpower Monthly*, Holland, March, 1990.

[37] Anon. Technical sheet of THERMIE project Renewables Wind Energy (RWE-8). OPET Sweden, Drottninggatan 50, 111 21 Stockholm, Sweden, Project end date: 1994-08-31. Contract no: WE/00010/91/DE.

[38] S. Mertens. The energy yield of roof mounted wind turbines. *Wind Engineering*, 27(6):507 – 518, 2003.

[39] A. D. Hansen, F. Iov, F. Blaabjerg, and L. H. Hansen. Review of contemporary wind turbine concepts and their market penetration. *Wind Engineering*, 28(3):247 – 263, 2004.

[40] S. Jöckel, A. Herrmann, and J. Rinck. High energy production plus built-in reliability - the Vensys 70/77 gearless wind turbines in the 1,5 MW class. Athens, Greece, 2006. European Wind energy Conference, EWEC 2006.

[41] E.F. Fuchs, A.A. Fardoun, P.W. Carlin, and R.W. Erickson. Permanent-magnet machines for operation with large speed variations. Seattle, USA, 1992. Proc. Of Windpower 1992.

[42] E. Spooner and A.C. Williamson. Direct coupled, permanent magnet generators for wind turbine applications. *IEE Proceedings of Electric Power Applications*, 143(1):1 – 8, 1996.

[43] M.A. Khan, P. Pilley, and M. Malengret. Impact of direct-drive WEC systems on the design of a small PM wind generator. volume 2, pages 7 – 14, Bologna, Italy, 2003. IEEE PowerTech Conference Proceedings.

[44] A. Grauers. Design of direct driven permanent magnet generators for wind turbines. ISBN 91-7197-373-7, Chalmers University of Technology, Gothenburg, Sweden, 1996. Ph.D. dissertation.

[45] P. Lampola. Directly driven, low-speed permanent-magnet generators for wind power applications. ISBN 951-666-539-X, Helsinki University of Technology, Finland, 2000. Ph. D. dissertation. Electrical Engineering series, No.101.

[46] P. Lampola. Losses in a directly driven, low-speed permanent-magnet wind generator. pages 358 – 364, Skagen, Denmark, 1996. Proc. of the Nordic Research Symposium on Energy Efficient Electric Motors and Drives.

[47] A. Grauers. Efficiency of three wind energy generator systems. *IEEE Transaction on Energy Conversion*, 11(3):650 – 657, 1996.

[48] M.A. Khan and P. Pillay. Design of a PM wind generator, optimised for energy capture over a wide operating range. pages 1501 – 1506, May, 2005. Proc. of Electric Machines and Drives, IEEE Int. Conf.

[49] H. Polinder, S.W.H. de Haan, M.R. Dubois, and J.G. Slootweg. Basic operation principles and electrical conversion systems of wind turbines. Trondheim, Norway, 2004. Proc. of the Nordic workshop on power and industrial electronics (NORPIE).

[50] M. Leijon and R. Liu. *Energy technologies: Electric power generators*, volume 3. Landolt-Börnstein, Springer Verlag, Germany, 2002. pages 151 – 164.

[51] E. Muljadi, C.P. Butterfield, and Y. Wan. Axial-flux modular permanent-magnet generator with a toroidal winding for wind-turbine applications. *IEEE transactions on Industry applications*, 35(4):831 – 836, 1999.

[52] B.J. Chalmers and E. Spooner. An axial-flux permanent-magnet generator for a gearless wind energy system. *IEEE Transactions on Energy Conversion*, 14(2):251 – 257, 1999.

[53] J. Chen, C.V. Nayar, and L. Xu. Design and finite-element analysis of an outer-rotor permanent-magnet generator for directly coupled wind turbines. *IEEE Transaction on Magnetics*, 36(5):3802 – 3809, 2000.

[54] E. Spooner, P. Gordon, J.R. Bumby, and C.D. French. Lightweight ironless-stator PM generators for direct-drive wind turbines. *IEE Proc. Electr. Power Appl.*, 152(1):17 – 26, 2005.

[55] M.R. Turner, R. Clough, H. Martin, and L. Topp. Stiffness and deflection analysis of complex structures. *J. Aero Sci.*, 23(9):805 – 823, 1956.

[56] T. Belytschko, W.K. Lin, and B. Moran. *Nonlinear finite elements for continua and structures*. John Wiley and sons Ltd., The Atrium, Southern Gate, Wichester, West Sussex P019 85Q, England, 2000.

[57] J.H. Argryris. Elasto-plastic matrix displacement analysis of three-dimensional continua. *J. Royal Aeronautical Society*, 69:633 – 635, 1965.

[58] P.V. Marcal and I.P. King. Elastic-plastic analysis of two dimensional stress systems by the finite element method. *Int. J. Mechanical Sciences*, 9:143 – 155, 1967.

[59] R.W. Clough. The finite element in plane stress analysis. Pittsburgh, Pennsylvania, USA, 1960. Proc. of $2^n d$ ASC conf. on Electronic Computation.

[60] J.L Volakis, A. Chatterjee, and L.C. Kempel. *Finite element method for electromagnetics*. IEEE Press, 445 Hoes Lane, P.O. Box 1331, Piscataway, NJ 08855-1331, p.37, 1998.

[61] A.Y. Hannalla and D.C. Macdonald. Numerical analysis of transient field problems in electrical machines. *Proc. Inst. Elec Eng.*, 123(9):893 – 898, 1976.

[62] A.Y. Hannalla. Analysis of transient problems in electrical machines allowing for end leakage and external reactances. *IEEE Transactions on Magnetics*, (2):1240 – 1243, 1981.

[63] A.B.J. Reece and T.W. Preston. *Finite element methods in electrical power engineering*. Oxford Univerity Press Inc., New York, USA, 2000.

[64] K. Hameyer and R. Belmans. *Numerical modelling and design of electrical machines and drives*. WIT Press, Southampton, UK, 1999.

[65] I.A. Tsukerman, A. Konrad, G. Meunier, and J.C. Sabonnadiere. Coupled field-circuit problems: Trends and accomplishments. *IEEE Transaction on Magnetics*, 29(2):1701 – 1704, 1993.

[66] C.A. Felippa. A historical outline of matrix structural analysis: a play in three acts. *Computers and Structures*, 79(14):1313 – 1324, 2001.

[67] T.L. Sullivan. A review of resonance response in large, horizontal-axis wind turbines. *Solar Energy*, 29(5):377 – 383, 1982.

[68] J. Wang, A. Elasser, E. Owen, J. Fogarty, and E. Kayicki. Electromechanical torsional analysis for a generator test bed. volume 2, pages 1028 – 1034. IEEE Industry Applications Conference, 37th IAS Annual Meeting, 2002.

[69] J.L. Peeters, D. Vandepitte, and P. Sas. Analysis of internal drive train dynamics in a wind turbine. *Wind Energy*, 9:141 – 161, 2005.

[70] Y.S. Lee and K.C. Hsu. Shaft torsional oscillation of induction machine including saturation and hysteresis of magnetizing branch with an inertia load. pages 134 – 139, Singapore, 1995. Proceedings of EMPD '95, IEEE International Conference on Energy Management and Power Delivery.

[71] T.J. Hammons and J.F. McGill. Comparison of turbine-generator shaft torsional responce predicted by frequency domain and time domain methods following worth-case supply system events. *IEEE Transactions on Energy Conversion*, 8(3):559 – 565, 1993.

[72] V. Akhmatov. Mechanical excitation of electricity-producing wind turbines at grid faults. *Wind Engineering*, 27(4):257 – 272, 2003.

[73] S.K. Salman and A.L.J. Teo. Windmill modeling consideration and factors influencing the stability of a grid-connected wind power-based embedded generator. *IEEE Transactions on Power Systems*, 18(2):793 – 802, 2003.

[74] M. Martins, A. Perdana, P. Ledesma, E. Agneholm, and O. Carlson. Validation of fixed speed wind turbine dynamic models with measured data. *Renewable Energy*, 32:1301 – 1316, 2007.

[75] S. Lefebvre and B. Dube. Control system analysis and design for an aerogenerator with eigenvalue methods. *IEEE Transactions on Power Systems*, 3(4):1600 – 1608, 1988.

[76] R.C. Reuter and M.H. Worstell. Torque ripple in a vertical axis wind turbine. Sandia National Laboratories, PO Box 5800, Albuquerque, NM 87185, USA, 1978. Sandia report SAND78-0577.

[77] J. Conroy and R. Watson. Torsional damping control of gearless full-converter large wind turbine generators with permanent magnet synchronous machines. *Wind Engineering*, 31(5):325 – 340, 2007.

[78] I. Paraschivoiu. *Wind turbine design with emphasis on Darrieus concept*. Polytechnic international press, Canada, 1st edition, 2002.

[79] P. Lorrain and D.R. Corson. *Electromagnetism: principles and applications*. W.H. Freeman and Company, New York, 2nd edition, 1997.

[80] J.J. Grainger and Jr. W.D. Stevenson. *Power system analysis*. McGraw-Hill, Inc., international edition, 1994.

[81] K-E. Hallenius. *Elektriska maskiner*. CWK Gleerup, Lund, Sweden, 1972.

[82] Edited by G. Elfving. *ABB Handbok Industri*. ABB Industrigruppen, Västerås, Sweden, 1993.

[83] A. Bedford W. and Fowler. *Dynamics: engineering mechanics*. Addison Wesley Longman, England, SI edition, 1996.

[84] H. Lundh. *Grundläggande hållfasthetslära*. KTH, Stockholm, Sweden, 3rd edition, 2000.

[85] A. Betz. *Windenergie und ihre ausnutzung durch windmüllen*. Vandenhoeck and Ruprecht, Gottingen, Germany, 1926.

[86] R. Gupta, R. Das, and K.K. Sharma. Experimental study of a Savonius-Darrieus wind machine. Washington, DC, USA, 2006. Proc. of Int. Conf. on Renewable Energy for Developing Countries.

[87] A. Broddefalk and M. Lindenmo. Dependence of the power losses of a non-oriented 3% Si-steel on frequency and gauge. *Journal of Magnetism and Magnetic Materials*, 304(2):e586 – e588, 2006.

[88] C. Mi, G.R. Slemon, and R. Bonert. Modeling of iron losses of permanent-magnet synchronous motors. *IEEE Transactions on Industry Applications*, 39(3):734 – 742, 2003.

[89] W. Chandrasena, P.G. McLaren, U.D. Annakkage, R.P. Jayasinghe, and E. Dirks. Simulation of eddy current effects in transformers. pages 122 – 126. IEEE CCECE 2002. Canadian Conference on Electrical and Computer Engineering, 2002.

[90] G. Bertotti. General properties of power losses in soft ferromagnetic materials. *IEEE Transaction on Magnetics*, 24(1):621 – 630, 1988.

[91] L. Ma, M. Sanada, S. Morimoto, and Y. Takeda. Prediction of iron loss in rotating machines with rotational loss included. *IEEE Transaction on Magnetics*, 39(4):2036 – 2041, 2003.

[92] A.J. Moses. Importance of rotational losses in rotating machines and transformers. *Journal of Materials Engineering and Performance*, 1(2):235 – 244, 1992.

[93] G. Diaz, C. Gonzalez-Moran, P. Arboleya, and J. Gomez-Aleixandre. Analytical interpretation and quantification of rotational losses in stator cores of induction motors. *IEEE Transactions on Magnetics*, 43(10):3861 – 3867, 2007.

[94] K. Atallah, D. Howe, P.H. Mellor, and D.A. Stone. Rotor loss in permanent magnet brushless ac machines. pages 60 – 62. Proc. of Electric Machines and Drives, Int. Conf. IEMD, 1999.

[95] G.J. Wakileh. Harmonics in rotating machines. *Electric Power Systems Research*, 66(1):31 – 37, 2003.

[96] G. Bedrosian. A new method for coupling finite element field solutions with external circuits and kinematics. *IEEE Transaction on Magnetics*, 29(2):1664 – 1668, 1993.

[97] F.A. Fouad, T.W. Nehl, and N.A. Demerdash. Permanent magnet modeling for use in vector potential finite element analysis in electrical machinery. *IEEE Transactions on Magnetics*, 17(6):3002 – 3004, 1981.

[98] R. Gupta, I. Yoshino, and Y. Saito. Finite element solution of permanent magnetic field. *IEEE Transactions on Magnetics*, 26(2):383 – 386, 1990.

[99] M.S. Sarma and J.C. Wilson. Accelerating the magnetic field iterative solutions. *IEEE Transactions on Magnetics*, (6):1042 – 1044, 1976.

[100] M. Ranlöf. Comparison of loss prediction methods under various excitation waveforms - numerical experiments, version 0.1. Internal report, Division for electricity, Box 534, 751 21 Uppsala, Sweden, 2008.

[101] Anon. Ace, modified version 3.1, ABB common platform for field analysis and simulations. ABB AB, Corporate Research, 721 78 Västerås, Sweden. ABB Corporate Research Centre.

[102] E. Brolin. Dimensioning and designing the structure and foundation of a h-rotor type wind turbine. Division for Electricity and Lightning Research, Box 534, 751 21 Uppsala, Sweden, 2006. Master Thesis work, UPTEC F06 045, Uppsala University.

Acta Universitatis Upsaliensis

Digital Comprehensive Summaries of Uppsala Dissertations from the Faculty of Science and Technology 547

Editor: The Dean of the Faculty of Science and Technology

A doctoral dissertation from the Faculty of Science and Technology, Uppsala University, is usually a summary of a number of papers. A few copies of the complete dissertation are kept at major Swedish research libraries, while the summary alone is distributed internationally through the series Digital Comprehensive Summaries of Uppsala Dissertations from the Faculty of Science and Technology. (Prior to January, 2005, the series was published under the title "Comprehensive Summaries of Uppsala Dissertations from the Faculty of Science and Technology".)

Distribution: publications.uu.se
urn:nbn:se:uu:diva-9210

ACTA
UNIVERSITATIS
UPSALIENSIS
UPPSALA
2008